JOURNAL OF GUIDANCE, CONTROL, AND DYNAMICS
Vol. 33, No. 3, May–June 2010

Online Aerodynamic Model Structure Selection and Parameter Estimation for Fault-Tolerant Control

T. J. J. Lombaerts,* E. R. Van Oort,† Q. P. Chu,‡ J. A. Mulder,§ and D. A. Joosten¶
Delft University of Technology, 2600 GB Delft, The Netherlands

DOI: 10.2514/1.47256

This paper describes a new recursive algorithm for the approximation of time-varying nonlinear aerodynamic models by means of a joint adaptive selection of the model structure and parameter estimation. This procedure is called adaptive recursive orthogonal least squares and is an extension and modification of the classical recursive orthogonal least-squares procedure. This algorithm is considered to be particularly useful for indirect fault-tolerant flight control, making use of model-based adaptive control routines. After the failure, a completely new aerodynamic model can be elaborated recursively with respect to structure, as well as parameter values. The performance of the identification algorithm is demonstrated on some simulation data sets.

Nomenclature

A_x, A_y, A_z	=	specific forces along the body's X, Y, Z axis, m/s^2
C	=	dimensionless coefficient
$\bar{c}$	=	mean aerodynamic chord, m
I	=	mass inertia, kg/m^2
L, M, N	=	total moment around the body's X, Y, Z axis, Nm
m	=	mass, kg
p, q, r	=	roll, pitch, and yaw rate around the body's X, Y, Z axis, rad/s
$\mathbf{Q}$	=	orthonormal matrix of **QR** decomposition
$\mathbf{R}$	=	upper triangular matrix of **QR** decomposition
S	=	wing area, m^2
u_b, v_b, w_b	=	airspeed velocity components along the body's X, Y, Z axis, m/s
u_n, v_n, w_n	=	airspeed velocity components along the Earth-fixed X, Y, Z axis, m/s
V	=	airspeed, m/s
X, Y, Z	=	total forces along the body's X, Y, Z axis, N
x, y, z	=	position coordinates along the X, Y, Z axis, m (reference frame varies)
$\mathbf{x}$	=	state vector
$\mathbf{z}$	=	dependent variable
$\mathbf{z}_m$	=	state measurement
α, β	=	angle of attack and sideslip angle, rad
δ	=	control surface deflection, rad
$\boldsymbol{\varepsilon}$	=	residual
$\boldsymbol{\theta}$	=	true parameter vector
$\hat{\boldsymbol{\theta}}$	=	estimated parameter vector
λ	=	forgetting factor
$\boldsymbol{\lambda}_b$	=	bias
$\boldsymbol{\nu}$	=	noise vector
$\hat{\boldsymbol{\xi}}$	=	residual vector
ξ	=	residual scalar
$\boldsymbol{\Pi}$	=	permutation matrix
ρ	=	air density, kg/m^3
$\boldsymbol{\Phi}$	=	data matrix with regressors or independent variables
ϕ	=	data matrix row with regressors or independent variables on one time instant
ϕ, θ, ψ	=	roll, pitch, and yaw angle, rad

Subscripts

a, e, r	=	aileron, elevator, and rudder
air, ail, aor, aol	=	inner right, inner left, outer right, and outer left ailerons
eir, eil, eor, eol	=	inner right, inner left, outer right, and outer left elevators
f_o, f_i	=	outer and inner flaps
i, k	=	variable number
i_h	=	incidence angle of the stabilizer, rad
l, m, n	=	total moment around the body's X, Y, Z axis, Nm
l, r	=	left and right
ru, rl	=	upper and lower rudders
s	=	subset
sp	=	spoiler

Presented as Paper 5725 at the AIAA Atmospheric Flight Mechanics Conference, Chicago, IL, 10–13 August 2009; received 18 September 2009; revision received 13 November 2009; accepted for publication 13 November 2009. Copyright © 2009 by Delft University of Technology. Published by the American Institute of Aeronautics and Astronautics, Inc., with permission. Copies of this paper may be made for personal or internal use, on condition that the copier pay the $10.00 per-copy fee to the Copyright Clearance Center, Inc., 222 Rosewood Drive, Danvers, MA 01923; include the code 0731-5090/10 and $10.00 in correspondence with the CCC.

*Ph.D. Researcher and Lecturer, Control and Simulation Division, Aerospace Engineering, P.O. Box 5058; t.j.j.lombaerts@tudelft.nl. Student Member AIAA.

†Ph.D. Researcher, Aerospace Software and Technologies Institute, Control and Simulation Division, Aerospace Engineering, P.O. Box 5058. Student Member AIAA.

‡Associate Professor, Control and Simulation Division, Aerospace Engineering, P.O. Box 5058. Member AIAA.

§Professor, Control and Simulation Division, P.O. Box 5058, Aerospace Engineering. Member AIAA.

¶Ph.D. Researcher, Delft Center for Systems and Control, P.O. Box 5058.

I. Introduction

BEING inspired by some recent aircraft accidents, fault-tolerant flight control (FTFC) is a control discipline in the aerospace community that is attracting an increasing amount of interest. FTFC is capable to reduce the number of aircraft accidents caused by loss of control in flight [1–7]. One of the methods to achieve FTFC is by applying so-called indirect adaptive control, in which a model-based adaptive control algorithm relies upon a real-time updated aerodynamic model of the damaged aircraft. Examples of this control method are nonlinear dynamic inversion [8], backstepping [9], or model predictive control [10,11]. This publication will focus on the postfailure identification of this aerodynamic model.

A number of aerodynamic model identification methods for FTFC have been proposed in the literature, like the use of indicial functions for unsteady aerodynamic effects [12], real-time identification in the frequency domain [13,14], and modified sequential least squares [15]. These publications demonstrate specific advantages for each

identification method. However, for these online methods, the conventional model structure is usually considered fixed, and the aerodynamic derivatives are deduced by means of some recursive or sequential least-squares procedure. However, this conventional structure may be especially invalid during highly dynamic maneuvers and in damaged situations. In these settings, it is highly probable that the conventional linear aircraft model structure must be extended with additional nonlinear and/or coupling terms and their accompanying derivatives. In this kind of application, one is not certain which independent variables may or may not have a significant influence on the dependent variable, which makes it important to apply some measure of structure selection. There are some good reasons for this. First of all, it complies with the principle of parsimony.

Definition 1: For the principle of parsimony, if there are two mathematical models to represent the same system with equal accuracy, then the model with the fewest parameters is preferable.

This principle promotes computational speed, which is especially important for online applications like those shown here. Another fact is that including a lot of insignificant data in the regressor set will lead to many small coefficients with large standard deviations, due to ill conditioning. Additionally, these coefficients, although small but numerous, perturb the estimation of the coefficients for the significant regressors.

Proof: Suppose the true system can be described as $\mathbf{z} = \Phi_{\text{sign}} \cdot \boldsymbol{\theta}$. Because of a lack of model structure information, its approximation is defined as follows:

$$\mathbf{z} = \Phi_{\text{sign}} \cdot \hat{\boldsymbol{\theta}}_{\text{sign}} + \Phi_{\text{insign}} \cdot \hat{\boldsymbol{\theta}}_{\text{insign}} \tag{1}$$

where Φ_{sign} contains the significant regressors and Φ_{insign} is the collection of insignificant regressors. Premultiplying Eq. (1) with $(\Phi_{\text{sign}}^T \Phi_{\text{sign}})^{-1} \Phi_{\text{sign}}^T$ results in

$$\hat{\boldsymbol{\theta}}_{\text{sign}} = \boldsymbol{\theta} - (\Phi_{\text{sign}}^T \Phi_{\text{sign}})^{-1} \Phi_{\text{sign}}^T \Phi_{\text{insign}} \hat{\boldsymbol{\theta}}_{\text{insign}} \tag{2}$$

which indicates a discrepancy between the parameter estimate $\hat{\boldsymbol{\theta}}_{\text{sign}}$ and the true parameter $\boldsymbol{\theta}$. This deviation becomes larger for $\hat{\boldsymbol{\theta}}_{\text{insign}}$ with a larger size if Φ_{sign} and Φ_{insign} are spanned in space by mutual linear dependent bases and Φ_{sign} is not well defined. There is no deviation if Φ_{sign} and Φ_{insign} are mutually orthogonal, which is generally not the case. □

Therefore, proper identification (including structure selection) is not avoidable for damaged aircraft with changed aerodynamic properties. In this paper, the aim of this routine is to perform adaptive structure selection and parameter estimation (SSPE) for an aerodynamic model of a structurally damaged aircraft. This allows the exploitation of the knowledge of these data for a model-based control technique; namely, adaptive nonlinear dynamic inversion (ANDI). In this way, safety and survivability will be enhanced. Earlier results of identification and FTFC investigations in this research project have been previously published [16–19]. This earlier work focuses on fixed model structures and offline structure selection. This paper highlights a new development; namely, online structure selection.

There are many interesting SSPE algorithms, like stepwise regression [20,21]. It is a very physical and intuitive procedure, but although it is not (yet) recursive, its main drawback is that it includes addition and elimination criteria. Therefore, it is less efficient than orthogonal least squares (OLS), which involve only a forward selection procedure. Especially for online applications, this is an important advantage. OLS have been used before for nonlinear modeling and roll derivatives estimation from flight data [22]. However, they have only been applied for batch data and not for damaged aircraft. For nonlinear aerodynamic modeling problems, the similar idea of generating multivariate orthogonal modeling functions from measured data, ranking those orthogonal functions by fit error reduction capability, and using the predicted square error (PSE) metric for model structure determination was originally developed by Morelli [23–25] and Klein and Morelli [26]. The PSE metric was originally developed earlier by Barron [27]. Moreover, orthogonal functions were used earlier by Mulder [28] in the optimization of multidimensional input signals for dynamic flight test maneuvers. However, this paper focuses on a new alternative approach via the working principle of OLS, which is computationally efficient for recursive applications.

The concept of recursive OLS (ROLS) has been introduced by Luo and Billings [29,31], Luo et al. [30], and Fung et al. [32] for which the concept of structure selection has been highlighted. This is a very interesting and powerful routine, which can also be applied for damaged aircraft model identification, as explained previously. However, for this aerospace application, some modifications are needed in the routine. Especially for online applications, it is important to include some protection against overfitting for computational speed and robustness considerations, which can be done by choosing an appropriate monitoring variable in the routine. Additionally, in damaged situations, the physical system model changes abruptly, and the routine must be rendered adaptive in order to deal with this varying structure. The objective of this paper is to solve these problems and to elaborate a basic routine, which is demonstrated for aerospace applications.

II. Principle of Orthogonal Least Squares

By augmenting the orthogonal decomposition techniques of the classical Gram–Schmidt (CGS) and the modified Gram–Schmidt [33], simple and efficient SSPE algorithms that determine Φ_s (a subset of Φ) can be derived in a forward regression manner by choosing one column of Φ for which the sum of squares of residuals is maximally reduced at a time in every step.

Assume that Φ_s has m_s ($m_s \leq m$ and $m_s < n$) columns, where m and n are the numbers of columns and rows of Φ, respectively. Factorize Φ_s into $\mathbf{Q}_s \mathbf{R}_s$, where $\mathbf{Q}_s$ is an $n \times m_s$ matrix consisting of m_s orthogonal columns and $\mathbf{R}_s$ is an $m_s \times m_s$ unit upper triangular matrix. This is commonly called a $\mathbf{QR}$ factorization. The residuals are defined by

$$\hat{\boldsymbol{\xi}} = \begin{bmatrix} \hat{\xi}(1) \\ \vdots \\ \hat{\xi}(N) \end{bmatrix} = \mathbf{z} - \Phi_s \hat{\boldsymbol{\theta}}_s = \mathbf{z} - \mathbf{Q}_s (\mathbf{R}_s \hat{\boldsymbol{\theta}}_s) = \mathbf{z} - \mathbf{Q}_s \mathbf{g}_s \tag{3}$$

Equation (3) can be rewritten as

$$\mathbf{z} = \mathbf{Q}_s \mathbf{g}_s + \hat{\boldsymbol{\xi}} \tag{4}$$

The sum of squares of the dependent variable $\mathbf{z}$ is, therefore,

$$\langle \mathbf{z}, \mathbf{z} \rangle = \sum_{i=1}^{M_s} g_i^2 \langle \mathbf{q}_i, \mathbf{q}_i \rangle + \langle \hat{\boldsymbol{\xi}}, \hat{\boldsymbol{\xi}} \rangle \tag{5}$$

The first term can be written as such, thanks to the properties of the orthogonal columns of $\mathbf{Q}_s$. The error reduction ratio (ERR) due to $\mathbf{q}_i$ is thus defined as the proportion of the dependent variable variance explained by $\mathbf{q}_i$:

$$[\text{ERR}]_i = \frac{g_i^2 \langle \mathbf{q}_i, \mathbf{q}_i \rangle}{\langle \mathbf{z}, \mathbf{z} \rangle} = \frac{g_i^2 \langle \mathbf{q}_i, \mathbf{q}_i \rangle}{\sum_{i=1}^{M_s} g_i^2 \langle \mathbf{q}_i, \mathbf{q}_i \rangle + \langle \hat{\boldsymbol{\xi}}, \hat{\boldsymbol{\xi}} \rangle} \tag{6}$$

Equation (6) suggests a way of computing $\mathbf{Q}_s$ (and hence Φ_s) from Φ by the CGS procedure. At the ith stage, by interchanging the i to m columns of Φ, we can select a $\mathbf{p}_i$ which gives the largest $[\text{ERR}]_i$ when orthogonalized into $\mathbf{q}_i$. The detailed procedure is as follows.

1) At the first step, for $1 \leq i \leq m$, compute

$$\mathbf{q}_1^{(i)} = \mathbf{p}_i \tag{7}$$

$$g_1^{(i)} = \frac{\langle \mathbf{q}_1^{(i)}, \mathbf{z} \rangle}{\langle \mathbf{q}_1^{(i)}, \mathbf{q}_1^{(i)} \rangle} \tag{8}$$

$$[\mathrm{ERR}]_1^{(i)} = \frac{(g_1^{(i)})^2 \langle \mathbf{q}_1^{(i)}, \mathbf{q}_1^{(i)} \rangle}{\langle \mathbf{z}, \mathbf{z} \rangle} \tag{9}$$

Find

$$[\mathrm{ERR}]_1^{(i_1)} = \max\{[\mathrm{ERR}]_1^{(i)},\ 1 \le i \le m\} \tag{10}$$

Select

$$\mathbf{q}_1 = \mathbf{q}_1^{(i_1)} = \mathbf{p}_{i_1} \tag{11}$$

2) At the kth step, where $k \ge 2$, compute for $1 \le i \le m$, $i \ne i_1, \ldots, i \ne i_{k-1}$:

$$\left.\begin{aligned} \alpha_{jk}^{(i)} &= \frac{\mathbf{q}_j^T \mathbf{p}_i}{\mathbf{q}_j^T \mathbf{q}_j} \\ \mathbf{q}_k^{(i)} &= \mathbf{p}_i - \sum_{j=1}^{k-1} \alpha_{jk}^{(i)} \mathbf{q}_j \end{aligned}\right\} \quad \text{for } 1 \le j < k \tag{12}$$

$$g_k^{(i)} = \frac{\langle \mathbf{q}_k^{(i)}, \mathbf{z} \rangle}{\langle \mathbf{q}_k^{(i)}, \mathbf{q}_k^{(i)} \rangle} \tag{13}$$

$$[\mathrm{ERR}]_k^{(i)} = \frac{(g_k^{(i)})^2 \langle \mathbf{q}_k^{(i)}, \mathbf{q}_k^{(i)} \rangle}{\langle \mathbf{z}, \mathbf{z} \rangle} \tag{14}$$

Find

$$[\mathrm{ERR}]_k^{(i_k)} = \max\{[\mathrm{ERR}]_k^{(i)},\ 1 \le i \le m,\ i \ne i_1, \ldots, i \ne i_{k-1}\} \tag{15}$$

3) Now select

$$\mathbf{q}_k = \mathbf{q}_k^{(i_k)} = \mathbf{p}_{i_k} - \sum_{j=1}^{k-1} \alpha_{jk}^{(i_k)} \mathbf{q}_j \tag{16}$$

4) The procedure is terminated at the m_s^{th} step when

$$1 - \sum_{j=1}^{m_s} [\mathrm{ERR}]_j < \rho \tag{17}$$

where $0 < \rho < 1$ is the chosen tolerance. This leads to a subset model containing m_s basis functions in the descending ordfer of dominance out of the m total basis functions.

The term

$$1 - \sum_{j=1}^{m_s} [\mathrm{ERR}]_j$$

is the proportion of the unexplained dependent variable variance. The value of ρ determines how many terms will be included in the final submodel. Generally, the appropriate value of ρ is found by trial and error and can vary between different categories of data sample stretches and regressors.

III. Principle of Adaptive Recursive Orthogonal Least Squares

ROLS are very similar to the classical OLS structure elaborated in Sec. II, but the procedure is rewritten in order to take into account a stepwise growing data matrix and vector of the dependent variable. SSPE by ROLS has been mentioned earlier by Luo et al. [30], but the adaptive ROLS (AROLS) algorithm is a new development. In this chapter, the differences between ROLS and AROLS are clearly shown. There are three crucial aspects that make AROLS different from regular ROLS. First, another subset selection stopping criterion has been chosen instead of the normalized residual sum of squares. The reason for this change is the fact that the other criterion is better suited to protect against overfitting, as will be shown later. Second, the procedure has been modified in order to deal with possible collinearities between the several regressors. Finally, a last step has been added to make the routine adaptable for changes in the dynamics of the true system. The advantages of AROLS are also illustrated in the application examples, shown in Sec. IV.

This recursive procedure is based upon the property that the columns in the $\mathbf{R}$ matrix of a $\mathbf{QR}$ decomposition can be interchanged arbitrarily and consecutively, as long as the product is compensated backward by a proper permutation matrix.

This property can be proven as follows.

Proof: Suppose that $\Phi = \mathbf{QR}$ and define $\mathbf{R}^{(1)} = \mathbf{R}\Pi_1$, where the permutation matrix Π_1 is orthonormal, so that $\Pi_1^{-1} = \Pi_1^T$. Correspondingly,

$$\mathbf{R} = \mathbf{R}^{(1)} \Pi_1^{-1} = \mathbf{R}^{(1)} \Pi_1^T \tag{18}$$

Because $\mathbf{R}^{(1)}$ is not purely upper triangular, it can be decomposed as

$$\mathbf{R}^{(1)} = \mathbf{Q}_N \mathbf{R}_N^{(1)} \tag{19}$$

Substituting all this for the original data matrix Φ results in

$$\Phi = \mathbf{QR}^{(1)} \Pi_1^T = \underbrace{\mathbf{Q}\mathbf{Q}}_{\substack{N \\ \mathbf{Q}^{(1)}}} \mathbf{R}_N^{(1)} \Pi_1^T \tag{20}$$

Now, define the second permutation:

$$\mathbf{R}_N^{(2)} = \mathbf{R}_N^{(1)} \Pi_2 \tag{21}$$

Correspondingly,

$$\mathbf{R}_N^{(1)} = \mathbf{R}_N^{(2)} \Pi_2^T \tag{22}$$

Because $\mathbf{R}_N^{(2)}$ is not purely upper triangular, it can once again be decomposed as

$$\mathbf{R}_N^{(2)} = \mathbf{Q}_{2N} \mathbf{R}_{2N}^{(2)} \tag{23}$$

Substituting all this for the original data matrix Φ results in

$$\Phi = \underbrace{\mathbf{Q}^{(1)} \mathbf{Q}_{2N}}_{\mathbf{Q}^{(2)}} \mathbf{R}_{2N}^{(2)} \underbrace{\Pi_2^T \Pi_1^T}_{\Pi_{\text{tot}}^T} \tag{24}$$

The principle holds by recursion for more permutations. □

Exploiting this property, the ROLS algorithm works generally as itemized next. For each item, references are given to the steps of the detailed procedure, which is given later.

1) Recursive orthogonalization occurs in steps 1 and 2.

2) Ranking according to capability for fit error reduction and stepwise addition to the subset occurs in steps 3 and 4.

3) Subset selection stopping criterion occurs in step 5.

4) Subset parameter estimation occurs in steps 6 and 7.

5) The subset selection necessity check occurs in step 8.

6) The reinitialization necessity check occurs in step 9.

In this general overview, it is important to realize that the criterion in step 8 triggers steps 4–6. If not needed, the subset selection steps are omitted, and the algorithm focuses on the parameter estimation task in step 7. On the other hand, steps 3–5 form a structure-ranking iteration procedure, which is terminated by the criterion in step 5. A visual overview of the procedure can be found in Fig. 1, in which a clear distinction is made between the standard steps to be performed under any circumstance (on the left) and the optional steps (on the right), of which the execution is triggered when needed. The detailed procedure of this algorithm is split up between an initialization phase and a recursive phase to be repeated for every time step.

Initialization:

For initialization, the $\mathbf{QR}$ decomposition generally works as follows:

$$\mathbf{z}(t) = \Phi(t)\boldsymbol{\theta}(t) + \boldsymbol{\nu}(t)$$

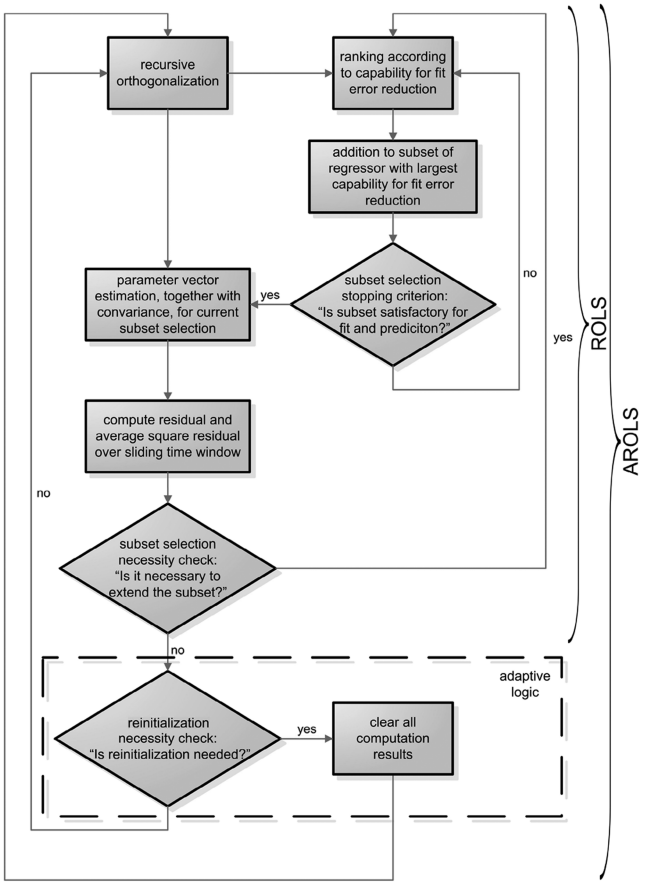

Fig. 1 Overview of the steps of the AROLS procedure.

$\Phi(t) = \mathbf{Q}(t)\mathbf{R}(t)$ with $\mathbf{Q}^T(t)\mathbf{Q}(t) = \mathbf{I}$, with $\mathbf{I}$ as the identity matrix and $\mathbf{R}(t)$ as the upper triangular.

Calculate $\mathbf{v}(t) = \mathbf{Q}^T(t)\mathbf{z}(t)$, because

$$\mathbf{v}(t) = \mathbf{Q}^T(t)\mathbf{z}(t) = \mathbf{R}(t)\boldsymbol{\theta}(t) + \mathbf{Q}^T(t)\boldsymbol{\nu}(t)$$

As initialization, the following initial values can be defined: $\mathbf{R}(t-1) = \mathbf{I}_m$ and $\mathbf{v}_m(t-1) = \mathbf{0}_{m\times 1}$.

Construct the augmented matrix:

$$\mathbf{R}_{\text{aug}}(t-1) = \begin{bmatrix} \mathbf{R}(t-1) & \mathbf{v}_m(t-1) \\ \mathbf{0}_1 & \mathbf{0}_2 \end{bmatrix}$$

$$\Pi_0 = \mathbf{I}_{m+1}$$

To be repeated for each of the following time steps:

1) Multiply this augmented matrix with the forgetting factor $\lambda^{1/2}$ and put the new data in a new row:

$$\mathbf{R}_{\text{aug}}(t) = \begin{bmatrix} [\lambda^{1/2}\mathbf{R}(t-1) & \lambda^{1/2}\mathbf{v}_m(t-1)] \\ [\phi_1(t), \ \dots, \ \phi_m(t) & z(t)]\Pi_{\text{tot}} \end{bmatrix} \tag{25}$$

2) Using Givens rotations, produce the new augmented matrix:

$$\mathbf{R}_{\text{aug}_{\text{new}}}(t) = \begin{bmatrix} \mathbf{R}(t) & \mathbf{v}_m(t) \\ \mathbf{0}_1 & \mathbf{0}_2 \end{bmatrix} \tag{26}$$

3) When the jth regressor is being selected, compute $v^2_{m(p)}(t)$, $p = j, \ \dots, \ m$, $j \geq 1$ based upon the updated values $\mathbf{v}_m(t)$ in Eq. (26) and choose the kth optimal regressor with the maximum $v^2_{m(p)}(t)$, $p = j, \ \dots, \ m$ for the jth position by earmarking the appropriate column of $\mathbf{R}(t)$.

4) This step can be skipped in the case that $j = k$.

According to the result from the previous step, as the kth variable has been selected, exchange the positions of the current jth and kth columns of $\mathbf{R}(t)$ and then retriangularize $\mathbf{R}(t)$ and rotate $\mathbf{v}_m(t)$ via $\mathbf{QR}$.** Mind that $j \leq k$. Define permutation matrix Π_{jk} accordingly:

$$\Pi_{jk} = \begin{bmatrix} \mathbf{I}_{j-1,j-1} & & & & \mathbf{0}_{j-1,m-k+1} \\ & 0_{j,j} & & 1_{j,k} & \\ & & \mathbf{I}_{k-j,k-j} & & \\ & 1_{k,j} & & 0_{k,k} & \\ \mathbf{0}_{m-k+1,j-1} & & & & \mathbf{I}_{m-k+1,m-k+1} \end{bmatrix}$$

and compute the total permutation matrix as the product of all individual permutation matrices $\Pi_{\text{tot}} = \prod(\Pi_{jk})$.

5) Evaluate a subset selection stopping criterion and perform the next step if this condition is satisfied; otherwise, return to step 3 to select more regressors. There are some alternatives for this subset selection stopping criterion, and this subject is elaborated further in a later stage.

6) Suppose that m_s regressors have been selected, then the computational augmented matrix is

$$\mathbf{R}_{\text{aug}}(t) = \begin{bmatrix} r_{11}(t) & \cdots & \cdots & r_{1,m_s}(t) & \cdots & r_{1,m-1}(t) & v_1(t) \\ 0 & \ddots & & \vdots & & \vdots & \vdots \\ \vdots & \ddots & \ddots & \vdots & & \vdots & \vdots \\ \vdots & & 0 & r_{m_s,m_s}(t) & & \vdots & v_{m_s}(t) \\ \vdots & & & 0 & \ddots & \vdots & \vdots \\ \vdots & & & \vdots & \ddots & r_{m-1,m-1}(t) & v_m(t) \\ 0 & \cdots & \cdots & 0 & \cdots & 0 & 0 \end{bmatrix} \tag{27}$$

7) A backsubstitution solver calculates the parameters $\hat{\theta}_i(t)$, $i = 1, \ \dots, \ m_s$ from $\mathbf{R}_{m_s}(t)$ [which is the top-left triangular portion of the final $\mathbf{R}_{\text{aug}}(t)$] and $\mathbf{v}_{m_s}(t)$, which consist of the first m_s elements of $\mathbf{v}_m(t)$. The standard deviation can be calculated by exploiting the property that

$$(\Phi_s^T\Phi_s)^{-1} = (\mathbf{R}_{m_s}^T\mathbf{Q}_s^T\mathbf{Q}_s\mathbf{R}_{m_s})^{-1} = (\mathbf{R}_{m_s}^T\mathbf{R}_{m_s})^{-1}$$

8) Compute the residual at the time instant t:

$$\boldsymbol{\varepsilon}(t) = \mathbf{z}(t) - \sum_{i=1}^{m_s} \boldsymbol{\phi}_i(t)\hat{\theta}_i(t)$$

This result is used to calculate the average square residual in the sliding time window M_s:

$$\bar{\varepsilon}^2_{M_s}(t) = \frac{1}{M_s}\sum_{i=0}^{M_s-1} \varepsilon^2(t-i)$$

with typically $M_s = 20$–100 (50 is chosen here). If the average square residual is below the predefined threshold $\bar{\varepsilon}^2_{M_s}(t) \leq \xi_{M_{s_1}} = 0.2$, then steps 4 to 6 can be omitted, and m_s remains unchanged. If the average residual exceeds the predefined threshold, steps 4 to 6 need to be performed again.

9) If the average square residual exceeds the second more relaxed threshold $\bar{\varepsilon}^2_{M_s}(t) \geq \xi_{M_{s_2}} = 0.3$ and if the standard deviation of all the coefficients is below a predefined third threshold $\sigma_j < \xi_{M_{s_3}}$,†† then all previous measurement data can be ignored, and the procedure has to start over again. The motivation for this is the fact that, for higher values of standard deviations, structure selection is most appropriate.

**Mind that calculating $\mathbf{Q}$ is not necessary here. All required information is contained in the upper triangular $\mathbf{R}$. This saves a considerable amount of computational load, especially because the size of $\mathbf{Q}$ increases with the number of data samples.

††This indicates a low level of uncertainty. Based upon the data content used until now, an accurate estimate has been obtained.

If the standard deviations are low and the average square residual exceeds a predefined threshold, one obtains an indication that the true system dynamics have changed when compared with the previous situation.

The last step can be omitted when one considers invariant nonlinear systems, like an aircraft performing a rapid maneuver in the same region of the flight envelope. However, when the nonlinear system can change suddenly in time (e.g., a damaged aircraft), one should ignore the data before the change, because they are not representative anymore for the actual current nonlinear system. This is the purpose of the last step.

The last remaining topic in this algorithm setup to be discussed is the subset selection stopping criterion. Several criteria can be used for this purpose. Klein and Morelli [26] mention, in this respect, the predicted sum of squares, the PSE, the coefficient of determination R^2, and the fit error. These metrics have been evaluated in the previous work of Lombaerts et al. [16]. It has been found that the PSE was preferable for offline applications of subset selection and parameter estimation on batch stretches of data, because of its clear optimum and its transparent breakup in an underfitting and an overfitting penalty term. The PSE can be calculated as follows. Compute the residual $\boldsymbol{\varepsilon}_{\mathbf{j}}$:

$$\boldsymbol{\varepsilon}_j(t) = \mathbf{z}(t) - \Phi(t) \cdot \Pi_{\text{tot}} \cdot \mathbf{R}(t)^{\dagger} \mathbf{v}_m(t) \tag{28}$$

where $\dagger$ represents the left inverse and $\sigma^2_{\max_N}$:

$$\sigma^2_{\max_N} = \frac{1}{N} \sum_{i=1}^{N} [z(i) - \bar{z}]^2 \tag{29}$$

Both are needed for the calculation of the PSE_j. This is a summation of two terms: the first one being the MSFE_j and the second one being an overfit penalty term (because it is proportional to the number of independent variables included in the regression p_j):

$$\text{PSE}_j = \underbrace{\frac{1}{N}(\boldsymbol{\varepsilon}_j^T \boldsymbol{\varepsilon}_j)}_{\text{MSFE}_j} + \sigma^2_{\max_N} \frac{p_N}{N} \tag{30}$$

In this expression, $\sigma_{\max_N}$ is an a priori upper-bound estimate of the squared error between the future data and the model. It should be noted that the PSE is particularly interesting for monitoring the progress of the routine, because it contains a data fitting as well as an overfit penalty term. This leads to a clear optimum, as can be seen in Fig. 2.

Verify if $\text{PSE}_{j-1} - \text{PSE}_j$ remains below a certain criticality threshold ϵ_{crit_1} (here, chosen as $\epsilon_{\text{crit}_1} = 1 \times 10^{-5}$) serves as a satisfactory subset selection stopping criterion. Application of this criterion for online applications has shown to work well for dimensionless forces of a significant magnitude (such as C_Z in the next example). However, it has been found that dimensionless moments (such as C_l and C_n in the next example) generally have lower orders of magnitude, leading to even lower MSFE values in the PSE criterion from the start onward. As a result, it has been observed in the experiments that the overfit penalty term has a higher relative weight, thus the use of the PSE for these types of dependent variables generally leads to an underfitted solution for the subset selection. Therefore, an alternative criterion has been searched for, which still has the same structure of a data fitting and an overfitting penalty term. Miller [34] gives a good overview of candidate critics. Possible candidates are listed next.

1) Akaike's Information Criterion (AIC) [35–37]:

$$\text{AIC}_j(\alpha) = N \ln(\text{MSFE}_j) + \alpha p; \qquad \alpha > 0 \tag{31}$$

2) The Schwarz criterion or Bayesian information criterion (BIC) [38] can be considered as a specific case of the AIC, where $\alpha = \ln(N)$, which is defined under the assumptions that the data distribution is in the exponential family. The BIC penalty term for additional parameters is stronger than that of the AIC:

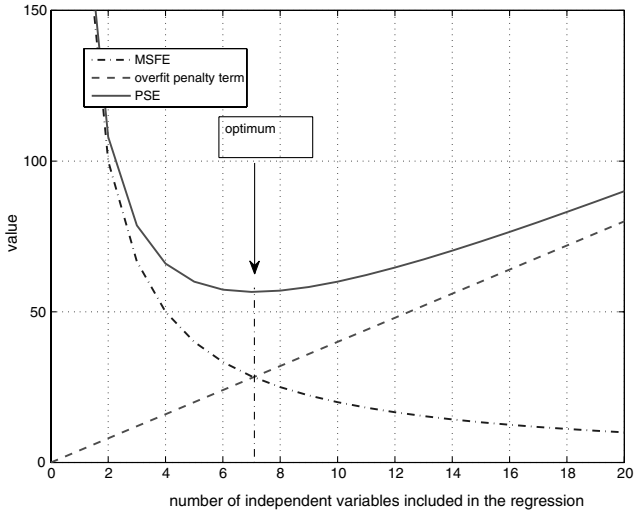

Fig. 2 Breakdown of the PSE in its data fitting and overfit penalty term (source: Klein and Morelli [26]).

$$\text{BIC}_j(\alpha) = N \ln(\text{MSFE}_j) + p \ln(N) \tag{32}$$

Because of its stronger penalty term, the BIC has been preferred for application in the AROLS algorithm. Experiments have shown that this criterion does not suffer from the previously mentioned underfitting tendency for the dimensionless moments, as occurs for the PSE. The same threshold principle has been used for this metric, as explained previously for the PSE.

The potential of this routine is shown in an example in the next section.

IV. Application for Identification of Time-Varying Aerodynamic Models Because of Failures

The application scenario is inspired by the so-called Bijlmermeer disaster of El Al flight 1862, for which a Boeing 747-200 cargo aircraft of Israel's national airline El Al lost two engines immediately after takeoff from the Schiphol Airport in Amsterdam, The Netherlands, and crashed into an apartment building in the neighborhood when trying to return to the airport. A detailed simulation model of this damaged aircraft is available from the National Aerospace Laboratory/NLR (The Netherlands). This reconfigurable control for vehicle emergency relief (RECOVER) benchmark model is discussed in detail by Smaili et al. [39,40] and has been used in the earlier publications of this research project but also in earlier versions by a number of investigators and organizations [10,41,42].

The simulation benchmark for evaluating fault-tolerant flight controllers, as discussed by Smaili et al. [39], contains six benchmark fault scenarios, enumerated in Fig. 3a. These failure cases have varying criticality. Figure 3b shows the failure modes and structural damage configuration of flight 1862's accident aircraft, which is the most important fault scenario in the simulation benchmark and is used in this application section. The RECOVER simulation model is an essential instrument in order to test the ability of the SSPE method to identify a damaged aircraft model in some realistic failure scenarios.

The El Al engine separation scenario is an accurate digital flight data recorder (DFDR) validated simulation of flight 1862, as explained previously, in which the loss of hydraulics is taken into account.

Before the actual joint structure selection and regression procedure can be applied, the governing dimensionless aerodynamic forces and moments need to be calculated as dependent variables.

A. Creating the Aerodynamic Forces and Moments

The calculation of the aerodynamic forces and moments can be done online, partly based upon the two-step method [28,43–45].

Failure mode	Reconfiguration	Criticality
No failure	N/A	None
Stuck or erroneous elevator	Stabilizer Ailerons (symmetric) Differential thrust	Major
Stuck or erroneous aileron	Ailerons (other) Spoilers	Major
Elevator/stabilizer runaway	Elevator Ailerons Flaps Thrust Use of static stability	Catastrophic
Stuck, erroneous or rudder runaway	Remaining surfaces Asymmetric thrust	Catastrophic
Loss of vertical tail surface	Differential thrust Differential speedbrakes	Catastrophic
Engine separation & structural damage	Remaining surfaces Remaining engines Remaining sensors	Catastrophic

a)

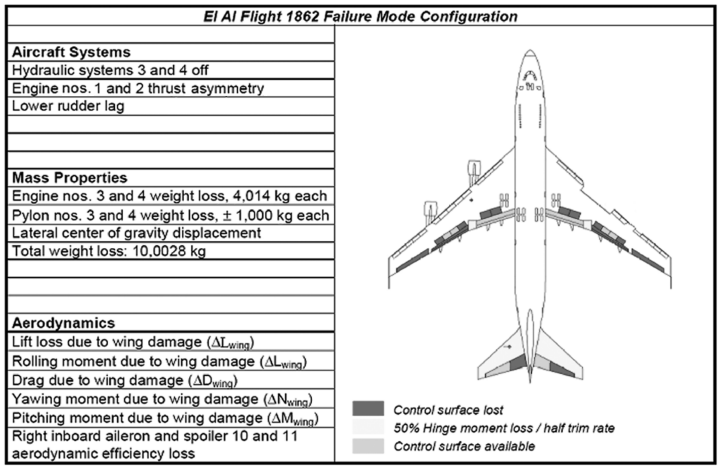

b) Failure modes and structural damage configuration of the Flight 1862 accident aircraft, suffering right wing engine separation, partial loss of hydraulics and change in aerodynamics

Fig. 3 Group for Aeronautical Research and Technology in Europe (GARTEUR) Flight Mechanics Action Group [FM-AG(16)] RECOVER benchmark simulation model [40]: a) benchmark fault scenarios and corresponding criticality, and b) configuration.

There are many other identification algorithms mentioned in the literature, like maximum likelihood identification and other one-step identification routines, but not all of them are applicable online. One of the few procedures that can be implemented in real time is the so-called filtering method developed at the DLR, German Aerospace Research Center [46]. This is a joint state and parameter estimation algorithm, but it is very complex. Another algorithm can be found in Morelli [47], which also works in real time and is frequency-based. In this context, one is looking for real-time physical parameter estimates in nonlinear models. Therefore, the two-step method seems to be the most appropriate and direct. One of the major advantages of the two-step method is the decomposition of a global nonlinear one-step identification method in two separate steps, as substantiated in Chu et al. [48], in which the nonlinear part is isolated in the aircraft state estimation step. The use of a Kalman filter in the first step makes it fairly straightforward to merge redundant but contaminated data, resulting in even higher accuracies. Consequently, the aerodynamic forces and moments can be calculated with the information obtained from the state estimation step.

1. *Aircraft State Estimation*

Estimating the aircraft states can be based upon redundant but contaminated information from all sensors. Standard available sensor information on civil airliners are classified in three categories. First, there are the air data sensors (ADS) providing TAS V_{TAS}, angle of attack α, and sometimes angle of sideslip β. Mind that most current-generation commercial transport aircraft do not directly measure sideslip angle but derive it from other parameters. However, this control strategy depends upon a direct independent measurement of β in order to detect errors in other parameters. For the purpose of FTFC, a more sophisticated ADS package needs to be implemented, including sideslip measurements. According to the authors, aircraft designs currently under development will have improved ADS equipment, some of them even including β sensors. A second class are the data from the inertial navigation system (INS) (consisting of inertial and magnetic equipment), giving measurement values for the specific forces A_x, A_y, and A_z, the rotational rates p, q, and r, and the aircraft attitude angles ϕ, θ, and ψ. The third, and last, category is a combination of INS and Global Positioning System (GPS) measurements, leading to data for the three-dimensional position x, y, and z and the inertial velocity components u_n, v_n, and w_n. At first sight, it looks that there is some redundancy in the velocity information, because the true airspeed V_{TAS}, the angle of attack α, and the angle of sideslip β also allow us to calculate the velocity components. However, it should be realized that these components are airspeed related, for which the inertial velocity components concern the ground speed. Comparing both sets leads to the derivation of the wind components. Table 1 gives information about the instrumentation errors that occur for each kind of measuring equipment mentioned previously. By making use of the kinematic and observation model of the aircraft, it is possible to estimate a part of the instrumentation errors, which will be discussed in more detail next.

Note from Table 1 that the computation of the true airspeed (TAS) requires measurement of the total pressure (pitot tube), the static pressure (static port), the total air temperature (TAT) probe, and the air density information (via altitude information) to convert the calibrated airspeed toward the TAS. Moreover, measurements of the angle of attack α and the sideslip angle β by the airflow angle vanes are perturbed by upwash, sidewash, and fuselage effects. In flight test practice, the observation model uses total air pressure p_t, static pressure p_s, TAT T_t [44], vane angle of attack α_v, and vane sideslip angle β_v [28] rather than V_{TAS}, α, and β. Biases and gain errors are estimated in this step. However, the research presented in this paper considers flight path reconstruction with a loosely coupled flight instrumentation system, using processed observations as opposed to the tightly coupled counterpart with raw measurement data.

The general state-space model set of nonlinear system equations describing the kinematics of the aircraft is given as follows:

$$\dot{\mathbf{x}}(t) = \mathbf{f}[\mathbf{x}(t),\ \mathbf{u}_m(t),\ \boldsymbol{\theta},\ t] + \mathbf{G}[\mathbf{x}(t)]\mathbf{w}(t); \qquad \mathbf{x}(t_0) = \mathbf{x}_0 \quad (33)$$

Table 1 Instrumentation error information for measuring equipment

Sensor	Variables	Bias error	Noise error
Translational accelerometer	A_x, A_y, A_z	✓	✓
Rate gyro	p, q, r	✓	✓
Integrating gyro	ϕ, θ, ψ	——	✓
INS/GPS	x, y, z	——	✓
INS/GPS	u_n, v_n, w_n	——	✓
Pitot tube, static port, TAT probe	V_{TAS}	——	✓
Airflow angle vane	α, β	——	✓

$$\mathbf{z}_m(t) = \mathbf{h}[\mathbf{x}(t),\ \mathbf{u}_m(t),\ \boldsymbol{\theta},\ t] + \mathbf{v}(t); \qquad t = t_i; \qquad i = 1,\ 2,\ \ldots \tag{34}$$

where Eq. (33) is known as the kinematic state equation with the input noise vector $\mathbf{w}$, and expression (34) is called the observation equation with the output noise vector $\mathbf{v}$. The nonlinear vector functions $\mathbf{f}$ and $\mathbf{h}$ may depend both implicitly (via $\mathbf{x}$ and $\mathbf{u}_m$) and explicitly on t, and it will be assumed that both $\mathbf{f}$ and $\mathbf{h}$ are continuous and continuously differentiable with respect to all elements of $\mathbf{x}$ and $\mathbf{u}_m$. The system equation variables are defined as follows:

$$\mathbf{x} = [\,x \quad y \quad z \quad u_b \quad v_b \quad w_b \quad \phi \quad \theta \quad \psi\,]^T \tag{35}$$

$$\mathbf{u}_m = \mathbf{u} + \boldsymbol{\lambda}_b + \mathbf{w} = [\,A_x \quad A_y \quad A_z \quad p \quad q \quad r\,]^T + [\,\lambda_x \quad \lambda_y \quad \lambda_z \quad \lambda_p \quad \lambda_q \quad \lambda_r\,]^T + \mathbf{w} \tag{36}$$

$$\boldsymbol{\theta} = [\,\boldsymbol{\lambda}_b \quad \mathbf{w}_{\text{wind}}\,]^T = [\,\lambda_x \quad \lambda_y \quad \lambda_z \quad \lambda_p \quad \lambda_q \quad \lambda_r \quad u_{\text{wind}} \quad v_{\text{wind}} \quad w_{\text{wind}}\,]^T \tag{37}$$

where the aircraft state vector $\mathbf{x}$ in Eq. (35) contains the inertial position, the body air velocity components, and the aircraft attitude angles. The measured input vector $\mathbf{u}_m$ in Eq. (36) consists of specific forces and angular rates perturbed with sensor biases and input noise, in which the sensor biases and wind ground speed components are collected in vector $\boldsymbol{\theta}$ in Eq. (37), which contributes for the augmented state vector as $\mathbf{x}_{\text{aug}} = [\mathbf{x},\ \boldsymbol{\theta}]$. Finally, there is the measured output vector $\mathbf{z}_m$ in Eq. (37), consisting of GPS-aided INS measurement data of position and velocity components (navigational frame of reference) and INS supplied attitude angles, as well as air data system measurements for TAS, angle of attack, and angle of sideslip. Also, the measured output vector is contaminated with output noise.

Additionally, the input noise vector $\mathbf{w}(t)$ is a continuous-time white noise process, and the output noise vector $\mathbf{v}(t_i)$ is a discrete time white noise sequence. Both are mutually uncorrelated, as well as between the different input and output channels individually. Moreover, based upon the known onboard measurement equipment characteristics, standard deviations are specified by the equipment manufacturers, taking into account some safety margins. Therefore, the error model can be described as follows:

$$\mathbf{v}(t_i) = [\,v_x \quad v_y \quad v_z \quad v_u \quad v_v \quad v_w \quad v_\phi \quad v_\theta \quad v_\psi \quad v_V \quad v_\alpha \quad v_\beta\,]^T \tag{39}$$

$$\mathbf{w}(t) = [\,w_x \quad w_y \quad w_z \quad w_p \quad w_q \quad w_r\,]^T \tag{40}$$

$$E\{\mathbf{w}(t)\mathbf{w}^T(\tau)\} = \mathbf{Q}\delta(t-\tau); \qquad \mathbf{Q} = \text{diag}(\sigma_{w_x}^2,\ \sigma_{w_y}^2,\ \sigma_{w_z}^2,\ \sigma_{w_p}^2,\ \sigma_{w_q}^2,\ \sigma_{w_r}^2) \tag{41}$$

$$E\{\mathbf{v}(t_i)\mathbf{v}^T(t_j)\} = \mathbf{R}\delta_{ij}; \qquad \mathbf{R} = \text{diag}(\sigma_{v_x}^2,\ \sigma_{v_y}^2,\ \sigma_{v_z}^2,\ \sigma_{v_u}^2,\ \sigma_{v_v}^2,\ \sigma_{v_w}^2,\ \sigma_{v_\phi}^2,\ \sigma_{v_\theta}^2,\ \sigma_{v_\psi}^2,\ \sigma_{v_V}^2,\ \sigma_{v_\alpha}^2,\ \sigma_{v_\beta}^2) \tag{42}$$

$$E\{\mathbf{w}(t)\mathbf{v}^T(t_i)\} = 0 \tag{43}$$

for

$$t = t_i; \quad i = 1,\ 2,\ \ldots$$

As already announced and apparent from the structure previously mentioned in this section, a Kalman filter can be used in order to estimate the aircraft states, the inertial sensor biases, and the wind velocity components.

2. *Calculating the Aerodynamic Forces and Moments*

The measurements and the Kalman filter states (more precisely, the aircraft states and the inertial measurement unit properties) are the available data for the next step. With this available information, it is possible to calculate the inertial measurements without bias, but the noise contribution cannot be compensated for. The key issue in this step is the determination of the aerodynamic forces and moments acting on the aircraft. Because these cannot be measured directly, it is possible to construct them with the help of the measurements of specific aerodynamic forces acting on the aircraft and angular rates and accelerations of the aircraft, which have already been corrected previously by means of the instrumentation errors (biases), as they were obtained in the aircraft state estimation step. In this way, the dimensionless forces and moments can be calculated as 1) dimensionless forces

$$\mathbf{z}_m = \left[\,x_{\text{GPS}} \quad y_{\text{GPS}} \quad z_{\text{GPS}} \quad u_{\text{GPS}} \quad v_{\text{GPS}} \quad w_{\text{GPS}} \quad \phi_{\text{INS}} \quad \theta_{\text{INS}} \quad \psi_{\text{INS}} \quad V_{\text{TAS}} \quad \alpha_{\text{ADS}} \quad \beta_{\text{ADS}}\,\right]^T \tag{38}$$

$$C_X = \frac{X}{1/2\rho V^2 S} = \frac{mA_x}{1/2\rho V^2 S}; \qquad C_Y = \frac{Y}{1/2\rho V^2 S} = \frac{mA_y}{1/2\rho V^2 S}; \qquad C_Z = \frac{Z}{1/2\rho V^2 S} = \frac{mA_z}{1/2\rho V^2 S} \tag{44}$$

and 2) dimensionless moments

$$C_l = \frac{L}{1/2\rho V^2 Sb} = \frac{\dot{p}I_{xx} + qr(I_{zz} - I_{yy}) - (pq + \dot{r})I_{xz}}{1/2\rho V^2 Sb}; \qquad C_m = \frac{M}{1/2\rho V^2 S\bar{c}} = \frac{\dot{q}I_{yy} + rp(I_{xx} - I_{zz}) + (p^2 - r^2)I_{xz}}{1/2\rho V^2 S\bar{c}}; \qquad C_n = \frac{N}{1/2\rho V^2 Sb} = \frac{\dot{r}I_{zz} + pq(I_{yy} - I_{xx}) + (qr - \dot{p})I_{xz}}{1/2\rho V^2 Sb} \tag{45}$$

At this moment, the mass and inertia are treated as known constants, because one considers only damaged aircraft with changed aerodynamic properties but no mass property changes in this stage. In the absence of a structural failure, the real-time mass and inertia can be calculated by integrating fuel flow and subtracting it from the total takeoff values. Future research is aimed at taking into account changing masses and inertia in the presence of structural failures. Air density can be deduced from altitude measurements. Decrease of measurement accuracy due to sensor failures in the ADS is ignored because of the assumed presence of sensor redundancy and sensor loss detection, which is usually the case. The rotational accelerations are obtained by differentiating the noisy rotational rates, which have been corrected for their biases. It should be noted that the current generation ring laser gyroscope noise levels are low enough ($\sigma_{pqr} = 0.001$ deg/s) to permit differentiating these signals. An alternative approach for estimating the rotary accelerations can be the use of two accelerometers with a known distance between them or direct measurements using angular acceleration sensors, such as the iMAR iODOT.[‡‡]

[‡‡]Data available online at http//www.imar-navigation.de [retrieved 13 Nov. 2009].

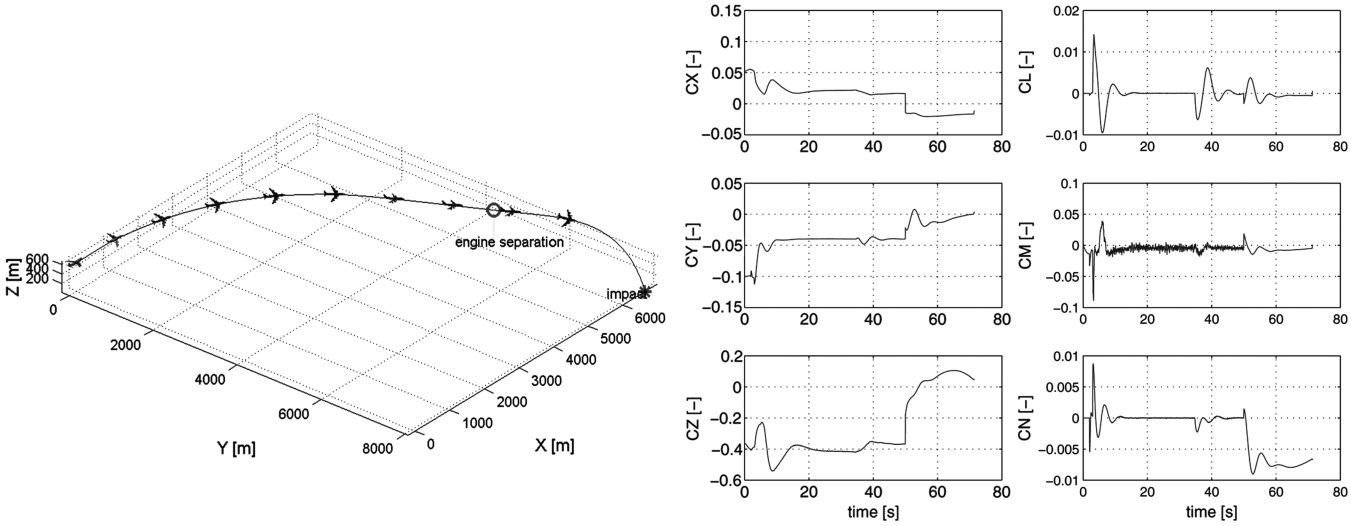

a) Simulation trajectory of engine separation scenario

b) Calculated dimensionless forces and moments coefficients during simulation

Fig. 4 Simulation information of the engine separation scenario.

Figure 4 shows the time histories of the calculated dimensionless forces and moments coefficients together with the corresponding trajectory of the simulated engine separation scenario. These data will be used for the application of AROLS in the subsequent section. The engine separation failure is triggered 50 s after the simulation started. Note that engine-related contributions in forces and moments are not included here. This study focuses exclusively on the aerodynamic effects.

B. Application of Adaptive Recursive Orthogonal Least Squares

As mentioned previously, the aerodynamic model structure must be selected while the model parameters are being estimated. This is one of the main advantages of the ROLS. Before this model structure selection can be set up, a pool of regressor candidates needs to be defined (i.e., independent variables which are candidates to be included in the structure).

As an example, the dimensionless force coefficient in the body's Z axis can be analyzed. Following the literature [21], the following independent variables can be treated as model regressor candidates. Despite the usual linear independent variables, which also occur in the regular aerodynamic models, there are also nonlinear symmetrical regressor candidates. In case of asymmetric damage, asymmetrical nonlinear regressor candidates also need to be taken into account. These three categories contain the following regressors:

1) The conventional linear independent variables are 1, α, $q\bar{c}/V$, and control surface deflections, such as δ_e.

2) The nonlinear symmetrical regressor candidates are α^2, α^m, $\alpha(q\bar{c}/V)$, and $\alpha\delta_e$, where $m = 3, \ldots, 8$.

3) The asymmetrical regressor candidates (linear, as well as nonlinear) are β, $pb/2V$, $rb/2V$, $\alpha\beta$, $\alpha\beta^2$, $\alpha^2\beta$, $\alpha\beta^3$, $\alpha^2\beta^3$, $\alpha(pb/2V)$, $\alpha(rb/2V)$, $\alpha^2(pb/2V)$, α^2, $rb/2V$, and β^n, where $n = 2, \ldots, 5$. Also, the dimensionless moment coefficients C_l and C_n can be analyzed. Taking into account the same categorization as previously, but this time for the lateral setup, one obtains the following:

1) The conventional linear independent variables are β, $pb/2V$, $rb/2V$, and control surface deflections, such as δ_a and δ_r.

2) The nonlinear asymmetrical regressor candidates are $\alpha\beta$, $\alpha\beta^2$, $\alpha^2\beta, \alpha\beta^3, \alpha^2\beta^3, \alpha(pb/2V), \alpha(rb/2V), \alpha^2(pb/2V), \alpha^2(rb/2V)$, and β^n, where $n = 2, \ldots, 5$.

3) The symmetrical regressor candidates (linear and nonlinear) are 1, α, $q\bar{c}/V$, α^2, α^m, $\alpha(q\bar{c}/V)$, and $\alpha\delta_e$, where $m = 3, \ldots, 8$.

Especially in the case of aircraft with a large set of control surfaces, like the Boeing 747, the possibility exists for identical or linear dependent control surface deflections (e.g., $\delta_{\text{eol}} = \delta_{\text{eor}}$ and $\delta_{\text{eil}} = \delta_{\text{eir}}$). However, it is still worthwhile to include them all in the regressor set, because the linear dependency can be lost after a control surface failure. Therefore, the choice has been made to include all of them in the candidate regressor set, but the maximum $v^2_{m(p)}(t)$ and $p \in \mathcal{P}$ in step 3 of the ROLS algorithm is only selected out of a subset $\mathcal{P}$, consisting of the columns corresponding with the remaining entries in a row reduced echelon form of the upper triangular matrix. In this way, one can avoid collinearities in the identification result.

As an example, the dimensionless force coefficient in the Z direction and the dimensionless moment coefficients C_l and C_n, as shown in Fig. 4b, have been selected as dependent variables to demonstrate the AROLS algorithm.

1. *Dimensionless Force Coefficient C_Z*

In this example, the dimensionless force coefficient C_Z is considered. First, the need for structure selection is illustrated. Predicting the dependent variable in postfailure conditions, based upon identification results in the unfailed situation, leads to the result as shown in Fig. 5a. From this figure, it is clear that the values related to the situation before the failure do not hold postfailure, as one would expect. Therefore, Fig. 5b illustrates the situation with the updated parameter value estimation restricted to the data after the failure but keeping the fixed conventional model structure, which was successful for fitting the data before the failure. This figure illustrates that the values are reestimated, but the algorithm is not successful in fitting the data set accurately without structure adaptation. This structure adaptation is exactly the purpose of AROLS, which will be illustrated in the remainder of this section.

Applying the AROLS routine to this stretch of simulation data leads to the results, as shown in Fig. 6. Figure 6a shows the results before failure, whereas Fig. 6b focuses on the postfailure situation. As can be seen in this figure, the fit is accurate. The optimal residual, which is updated over the entire time history at every time step, is minimal. The real residual, which is not updated a posteriori, gives an indication of the reduction in the residual over the time interval. Figure 6a reveals the initial large residual due to initialization. Figure 6b shows the initial large residual caused by the failure. This is minimized in a very short term, but it starts increasing thereafter due to slow dynamics that become dominant. Between 55 and 60 s, the residual is again minimized, thanks to the incorporation of these slow dynamics in the aerodynamic model.

The parameter estimation results, together with their standard deviations, can be found in Table 2. These results highlight the difference between the situations before and after failure. Because there is no anomaly before the failure, the important independent variables for the vertical force are the conventional ones; namely, a constant, the angle of attack α, and the pitch rate $q\bar{c}/V$. However,

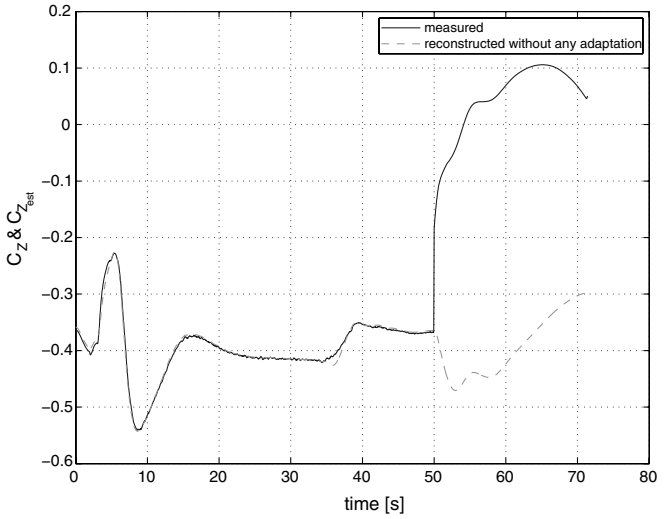

a) Fitting with originally selected structure and estimated parameter values for the unfailed situation

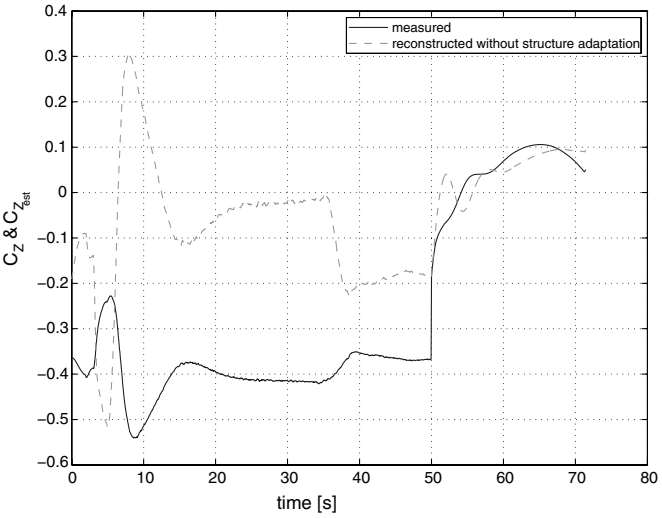

b) Fitting with originally selected structure for the unfailed situation but with updated estimated parameter values for the failed situation

Fig. 5 Fitting of complete data set of C_Z without full adaptation for the postfailure characteristics

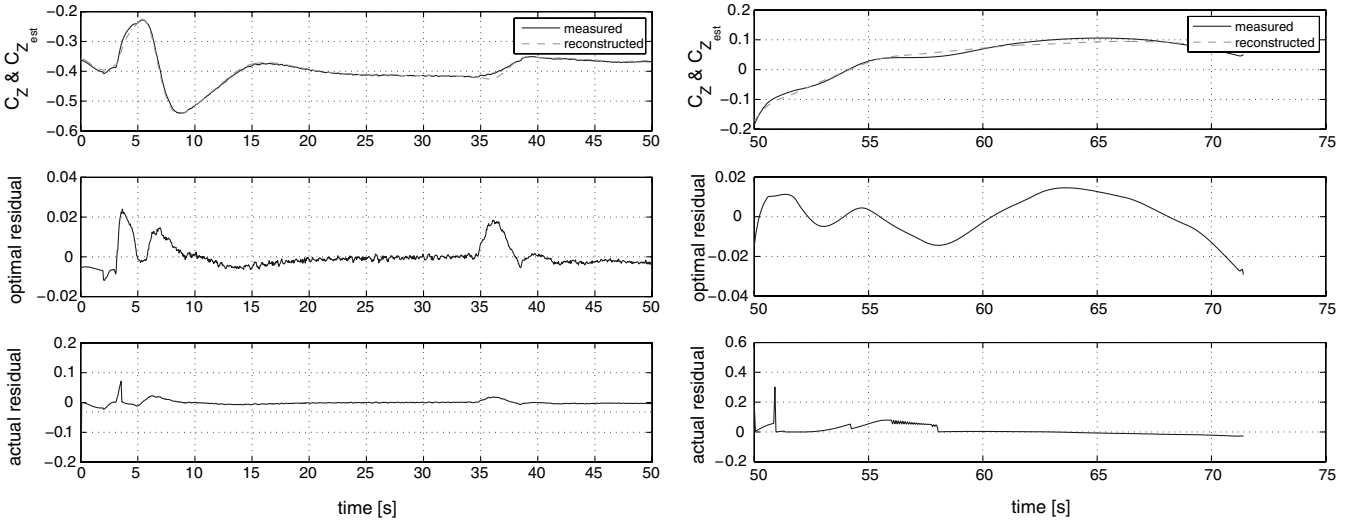

a) **b)**

Fig. 6 AROLS SSPE results for C_Z: a) before and b) after the failure.

after the failure, a violent roll–dive maneuver follows. The influence of the damage on the change in aerodynamics is represented by additional contributions by sideslip β and roll rate $pb/2V$. These are clearly a consequence of the asymmetric damage, as a result of which the decoupling of longitudinal and lateral regressors does not hold anymore in this scenario. The standard deviations give an indication of the accuracy of the results.

The development of the structure selection algorithm can be seen in Fig. 7. Figure 7a shows the number of regressors, which have been included, and Fig. 7b displays the time history of the monitoring criteria. The first few seconds of the simulation, the initialization takes place although there is no significant excitation or dynamics, after which only one regressor (being the constant) is selected, which is sufficient to represent the aerodynamic model during these first few seconds. Between 5 and 10 s, a dynamic right-hand turn is executed, which leads to an extension of the model structure because of the significant excitation. Soon after the start of the turn, a repetition of the structure selection phase is triggered, and at the end, the three conventional regressors are retained. Because the mean-squared residual, shown in Fig. 7b, does not cross the first threshold $\xi_{M_{s_1}}$ anymore afterward, the structure selection is frozen after this phase, which saves a considerable amount of computational load and time. When the engines separate, $\bar{\varepsilon}^2_{M_s}(t)$ increases dramatically, whereas the maximum standard deviation remains below its threshold $\xi_{M_{s_3}}$. This triggers step 9 in the ROLS algorithm, and the identification procedure is reset, ignoring all data collected before, because they have become irrelevant for the new configuration. During the first few seconds, there is a brief transient, because the algorithm tries first to fit the new aircraft behavior by extending the regressor subset without resetting the data content. But, thereafter, the reinitialization

Table 2 SSPE results for C_Z for engine separation scenario (before and after failure)

	Prior failure		Postfailure	
	Estimated	σ	Estimated	σ
1	−0.1583	0.0010	−0.4131	0.0084
α	−4.4016	0.0216	4.9047	0.0272
$(q\bar{c}/V)$	−1.6124	0.3563	105.1966	1.4089
β	0	0	4.2319	0.0272
$(pb/2V)$	0	0	9.4708	0.0084
$(rb/2V)$	0	0	0	0
All others	0	0	0	0

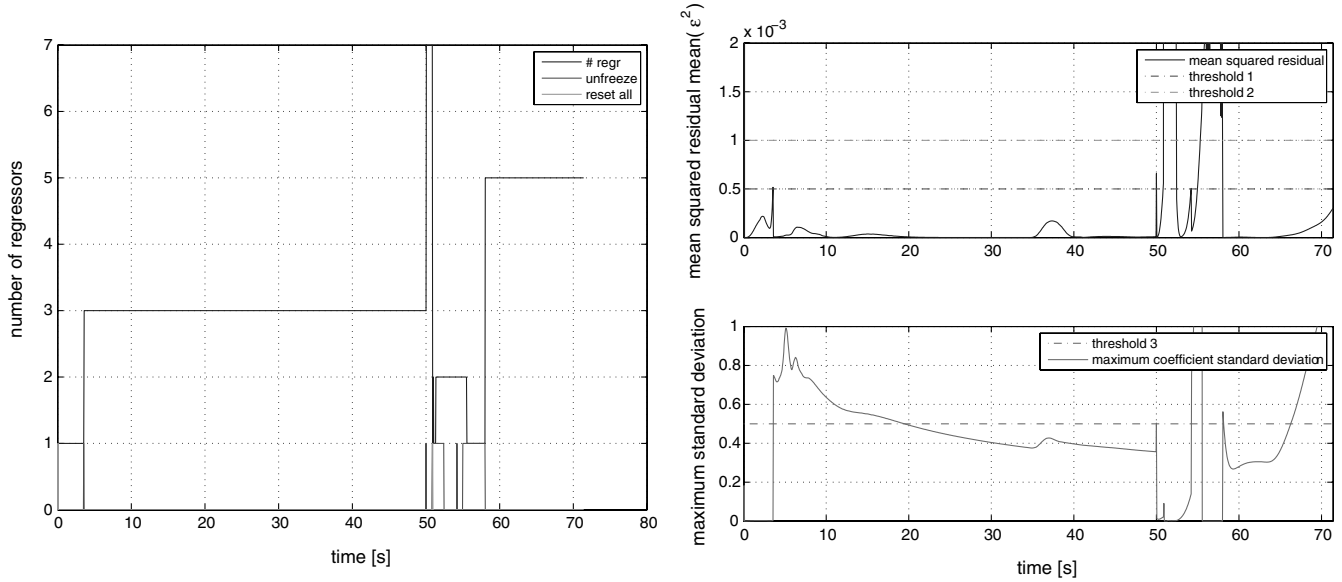

Fig. 7 C_Z: a) number of regressors included and b) triggering of structure selection procedure and parameter estimation result after failure.

is triggered and only two regressors are retained; namely, $q\bar{c}/V$ and $pb/2V$ are included, because they represent the fastest dynamics, which are dominant in the short term. However, slower dynamics are not yet present at that time instant but become apparent in the subsequent seconds, from 53 s onward. This influence makes the mean-squared residual increase and triggers the structure selection routine again around $t = 58$ s, because the standard deviation values are too large to warrant a new reinitialization. In the subsequent structure selection steps, the slower regressors 1, α, and β are included simultaneously. After this, the structure selection procedure freezes again completely, because $\bar{\varepsilon}^2_{M_s}(t)$ becomes extremely small, well below threshold $\xi_{M_{s_1}}$. However, it can once again be seen that, toward the end, the mean-squared residual increases again, due to new slower dynamics (which become influential) and will unfreeze the selection once again. However, the aircraft impacts terrain and the simulation is terminated before this new structure selection step is triggered.

Figure 8 shows the AROLS results over the complete time span. The optimal residual is updated over the entire time history at every time step, as explained before. The real residual on the contrary is the actual residual at every time step, without a posteriori update. Except for two major exceptions, namely initializations in the beginning of the simulation and after failure, this real residual is very small and confirms the accuracy of structure and parameter estimates. However, the optimal residual has an additional monitoring purpose. For this specific example, there is an abrupt change, and the change in model structure is relatively quickly detected by means of the

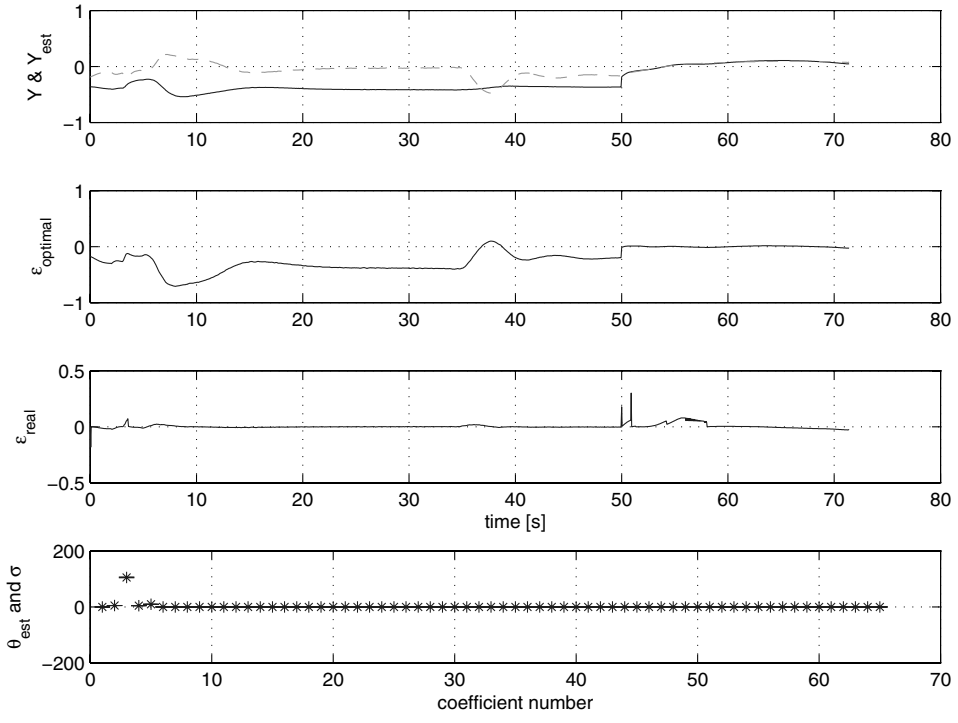

Fig. 8 Results of AROLS over a complete time span for C_Z. (Solid lines denote true and dashed lines denote final AROLS result.)

monitoring criteria, which also reveals approximately when the failure occurred (here, at $t = 52$ s). However, it is also possible that some gradual developing failures occur. The time instant when the reset operation is triggered by the monitoring criteria can be significantly later, hiding the true time instant when the failure occurred. In these scenarios, the optimal residual has an additional advantage, because it will reveal when the failure occurred. More precisely, the time instant in which the optimal residual changes from substantial to extremely small corresponds to the moment of failure. In Fig. 8, this corresponds to $t = 50$ s.

Figure 9 serves as an additional validation test, in which the vertical specific force A_z is calculated with the SSPE result, before and after the failure, and compared with the measured value. Note that these results have been obtained without mass updates but with the original values, which are biased in postfailure conditions. This validation confirms the accuracy of the achieved identification result, including structure selection. Moreover, the significant difference between the situations before and after failure can be observed in this figure.

2. *Dimensionless Moment Coefficient C_l*

Applying the AROLS routine to this stretch of simulation data leads to the results, as shown in Fig. 10. Also, for this example, the fit is accurate. Especially after the failure, the real residual illustrates that the structure selection procedure is triggered whenever it deviates significantly from zero.

The parameter estimation results, together with their standard deviations, can be found in Table 3. These results highlight the difference between the situations before and after failure. Because

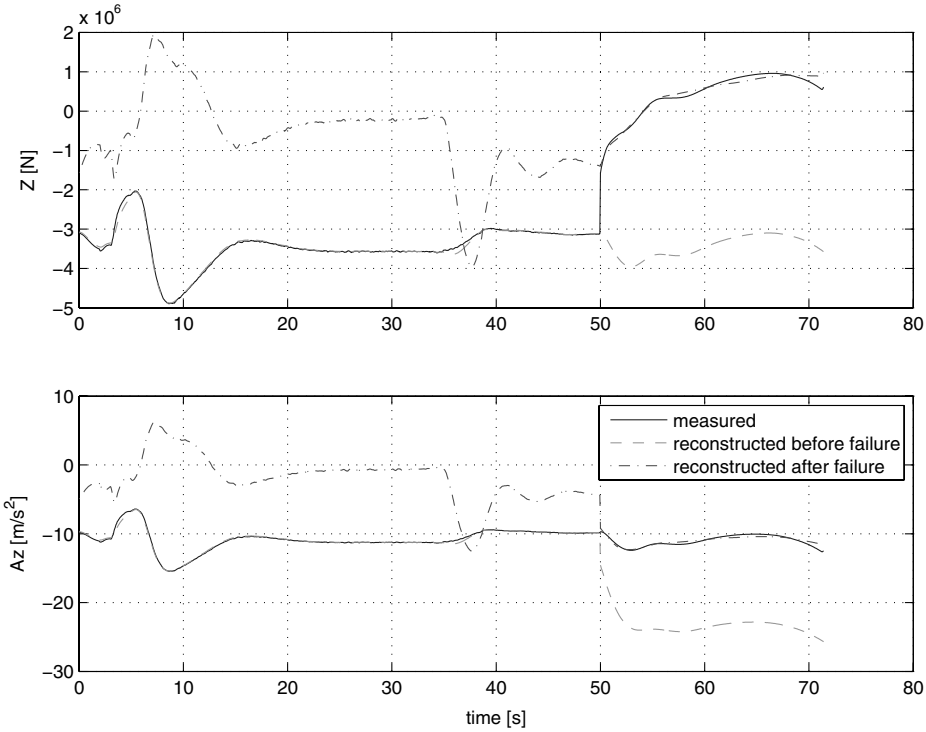

Fig. 9 Reconstruction of the vertical specific force A_z with the SSPE result.

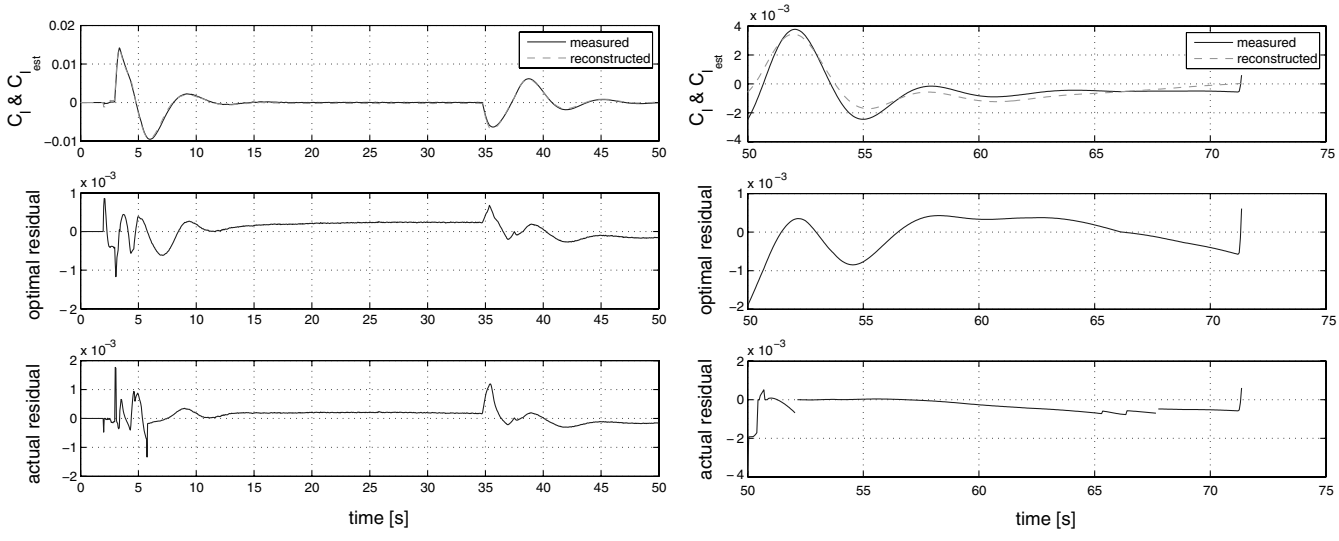

a) b)

Fig. 10 AROLS SSPE results for C_l: a) before the failure and b) after the failure.

Table 3 SSPE results for C_l for engine separation scenario (before and after failure)

	Prior failure		Postfailure	
	Estimated	σ	Estimated	σ
β	−0.1130	0.0016	−0.1673	0.0015
$(pb/2V)$	−0.3109	0.0011	−0.3065	0.0025
$(rb/2V)$	0	0	0	0
δ_{air}	−0.0005	1.2e − 5	0	0
δ_{ail}	0	0	0	0
δ_{aor}	−0.0004	4e − 6	0	0
δ_{aol}	0.0003	4e − 6	0	0
1	0	0	0	0
α	0	0	0	0
$(q\bar{c}/V)$	0	0	−0.4706	0
All others	0	0	0	0

there is no anomaly before the failure, the important independent variables for the rolling moment are the conventional ones; namely, the angle of sideslip β, the roll rate $pb/2V$, and the ailerons as control effectors. Recall that the inner left aileron $\delta_{a_{\text{IL}}}$ is not included, because its deflection is collinear with another aileron surface. This is achieved by considering the row reduced echelon form. However, after the failure, a violent roll–dive maneuver follows, as illustrated previously. The influence of the damage on the change in aerodynamics is represented by an additional contribution from pitch rate $q\bar{c}/V$, because decoupling of longitudinal and lateral regressors does not hold anymore in this scenario. It should also be noted that the ailerons are not significant regressors after the failure. This is because they cannot move anymore, as can be seen in Fig. 3. A few spoilers remain effective, but these are not sufficiently excited by the classical control system in this short time span to allow a successful identification of their individual control efficiencies. Therefore, separate surface excitation is needed [49,50]. In combination with the SSPE algorithm, this will provide reliable values for the primary control efficiencies. Subsequently, this information can be used by the model-based control algorithm, such as ANDI.

The development of the structure selection algorithm is again displayed in Fig. 11. Figure 11a shows the number of regressors that have been included, and Fig. 11b displays the time history of the monitoring criteria. Between 5 and 10 s, when the dynamic right-hand turn is executed, the rolling moment is excited significantly, and the model structure is extended accordingly. Soon after the start of the turn, a repetition of the structure selection phase is triggered and, at the end of the turn, the structure is frozen and will not change anymore until the failure occurs. When the engines separate, $\bar{\varepsilon}^2_{M_s}(t)$ increases dramatically, whereas the maximum standard deviation shows no significant increase. This triggers step 9 in the ROLS algorithm, and the identification procedure is reset, ignoring all data collected before because they have become irrelevant for the new configuration. The reinitialization is triggered and, after some model development updates, only three regressors are retained; namely, β, $pb/2V$, and $q\bar{c}/V$ are included, because they represent the most important dynamics, which are dominant in the longer term. Initially, the yaw rate $rb/2V$ is also included, but its relevance (together with its coefficient) decreases over time, and the regressor becomes redundant from 68 s onward. After this, the structure selection procedure freezes again, because $\bar{\varepsilon}^2_{M_s}(t)$ becomes smaller again (but not far below threshold $\xi_{M_{s_1}}$), pointing out that an optimal fit has not yet been achieved. Toward the end, it can also be seen that the mean-squared residual increases again, due to new slower dynamics that become influential. These dynamics would unfreeze the selection once again if the aircraft would not have hit terrain.

Figure 12 shows the AROLS results over the complete time span. The optimal and real residuals have been defined in the previous example. The upper graph illustrating the true signal and its final approximation, after failure and at the moment of impact, fits the postfailure data well but not the stretch of data before the failure. This illustrates the significant difference in model properties before and after failure and, thus, the extent of the damage and its influence on the aircraft behavior.

An additional validation test is provided in Fig. 13, in which the roll acceleration $\dot{p}$ is calculated by means of the SSPE result, before and after the failure, and compared with the measured value. Note that these results have been obtained without postfailure mass updates. The accuracy of the achieved identification result is confirmed by this test. Moreover, in comparison with the previous application example, there is still some difference between the situations before and after failure (as can be observed in this figure), but the difference is less significant. The largest difference can be observed immediately after failure.

3. *Dimensionless Moment Coefficient C_n*

Figure 14 shows the results of AROLS applied to this stretch of data. As can be seen in this figure, the fit is accurate once again.

The parameter estimation results, together with their standard deviations, can be found in Table 4. Before the failure, the important

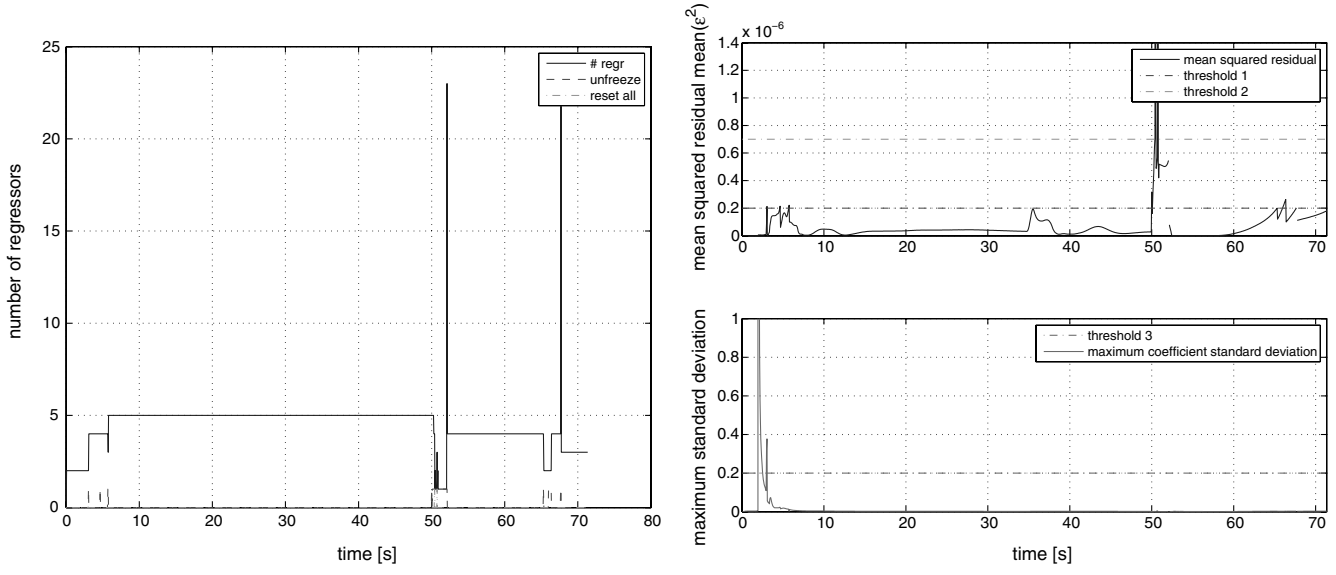

a) b)

Fig. 11 C_l: a) number of regressors included and b) triggering of structure selection procedure and parameter estimation result after failure.

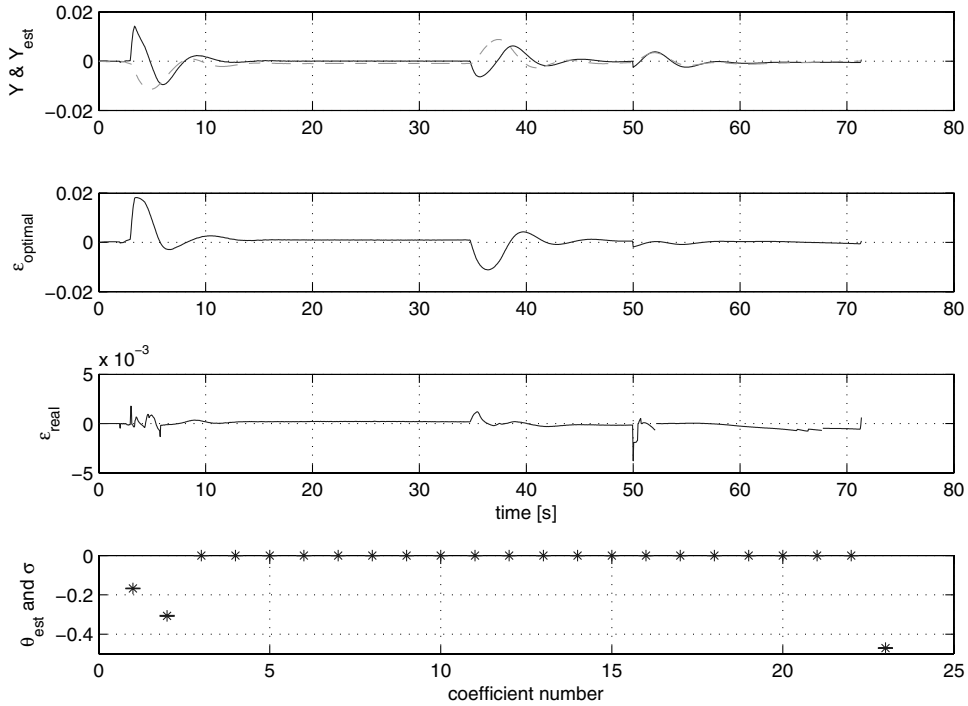

Fig. 12 Results of AROLS over complete time span for C_l. (Solid lines denote true and dashed lines denote final AROLS result.)

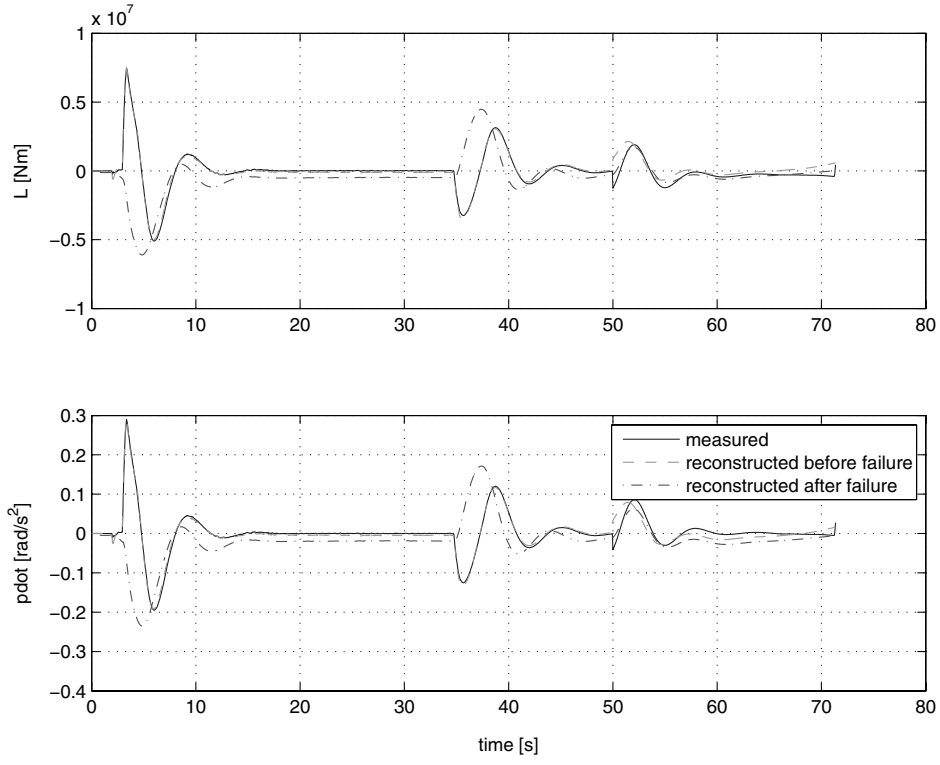

Fig. 13 Reconstruction of the roll acceleration $\dot{p}$ with the SSPE result.

independent variables for the yawing moment are the conventional ones; namely, the angle of sideslip β, the roll rate $pb/2V$, the yaw rate $rb/2V$, and the ailerons and rudder as control effectors. As one would expect, the rudder is the most efficient yawing control effector, and this can be seen in the estimated value, which is an order of magnitude larger when compared with the aileron effectiveness. After the failure, a violent roll–dive maneuver follows, but surprisingly, there is no difference in model structure between the situations before and after failure. Comparing the estimated values before and after failure shows that there is little change in the influence of the independent variables on the yawing moment. Apparently, the influence of the damage can be found primarily in the rolling moment L, and it is minimal on the yawing moment N. Recall that asymmetric thrust is not taken into account here, only the aerodynamic moment is considered. Wing damage has clearly more effect on the rolling moment L than on the yawing moment N. The latter can be influenced more effectively by damage to the vertical tail, for example.

The development of the structure selection algorithm can be seen in Fig. 15. No special observations occur here. During the right-hand

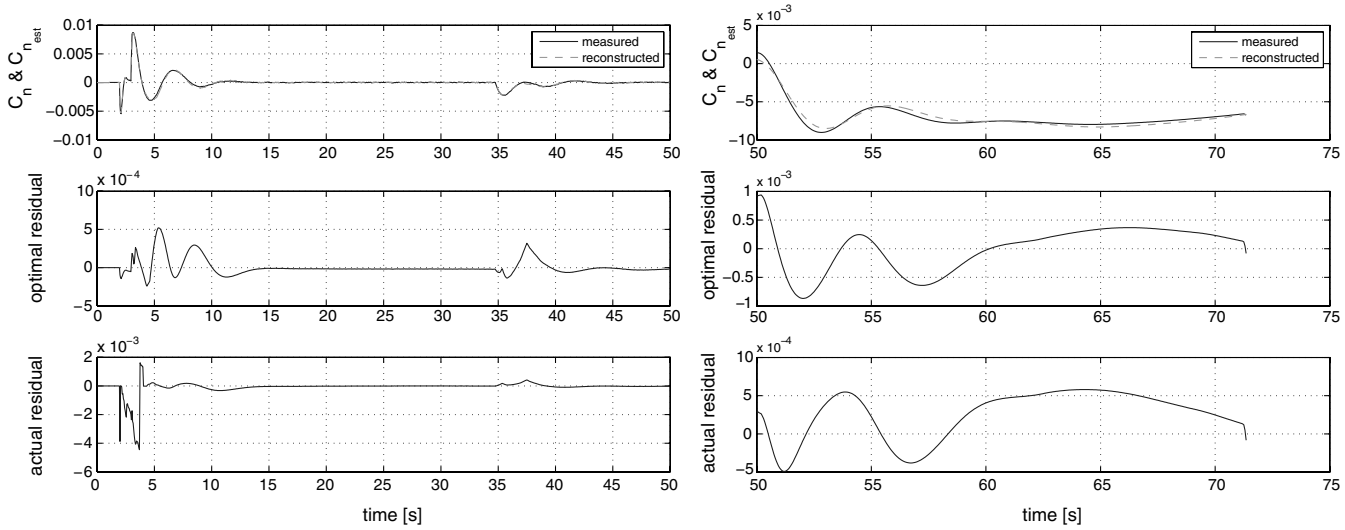

Fig. 14 AROLS SSPE results for C_n: a) before the failure and b) after the failure.

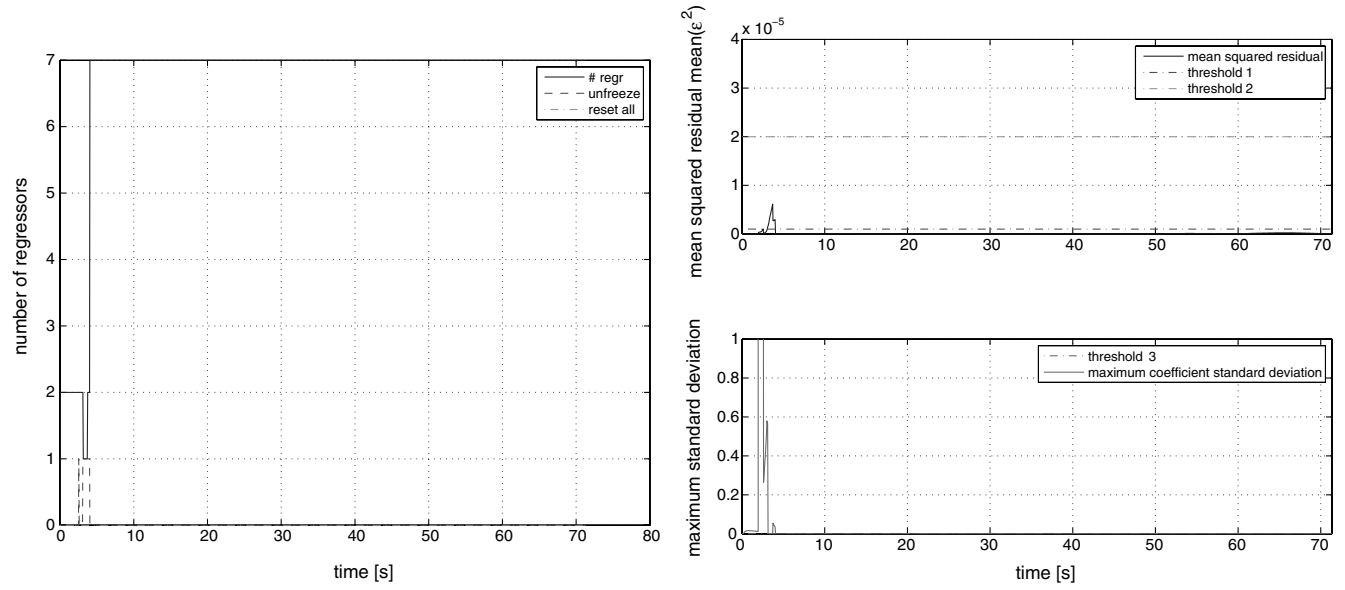

Fig. 15 C_n: a) number of regressors included and b) triggering of structure selection procedure and parameter estimation result after failure.

Table 4 SSPE results for C_n for engine separation scenario (before and after failure)

	Prior failure		Postfailure	
	Estimated	σ	Estimated	σ
β	0.1385	1.9e − 5	0.1257	6.5e − 5
$(pb/2V)$	−0.0249	3.1e − 5	−0.0252	6.5e − 5
$(rb/2V)$	−0.1953	2.3e − 5	−0.1763	7.4e − 5
δ_{air}	−0.0001	0	−0.0002	0
δ_{ail}	0	0	0	0
δ_{aor}	−0.0001	1.4e − 5	2.7e − 7	2.8e − 5
δ_{aol}	−1.2e − 6	1.3e − 5	−2.1e − 5	1.9e − 5
δ_{rl}	−0.0015	1.9e − 5	−0.0015	4.3e − 5
δ_{ru}	0	0	0	0
All others	0	0	0	0

turn, the model structure is selected and does not change anymore afterward until impact with the terrain. This is underpinned by the time history of the value of the mean-squared residual, which remains small at any time.

Figure 16 shows the AROLS results over the complete time span. The upper graph confirms that there is no significant change in the yawing moment characteristics between situations before and after damage. The fitting result at the end fits the complete data set very well, from the initial situation till the end. This confirms that an SSPE procedure is not needed for this specific dependent variable, which is taken into account by the AROLS algorithm, because a reinitialization is not activated.

Analogously, as in the previous examples, Fig. 17 serves as validation. It is most important to take into account the important thrust contribution for N in this test. Note that these results have also been obtained without postfailure mass updates. Once again, the accuracy of the achieved identification result is confirmed by this test. Moreover, in contrast with the previous application examples, there is no significant difference between the situations before and after

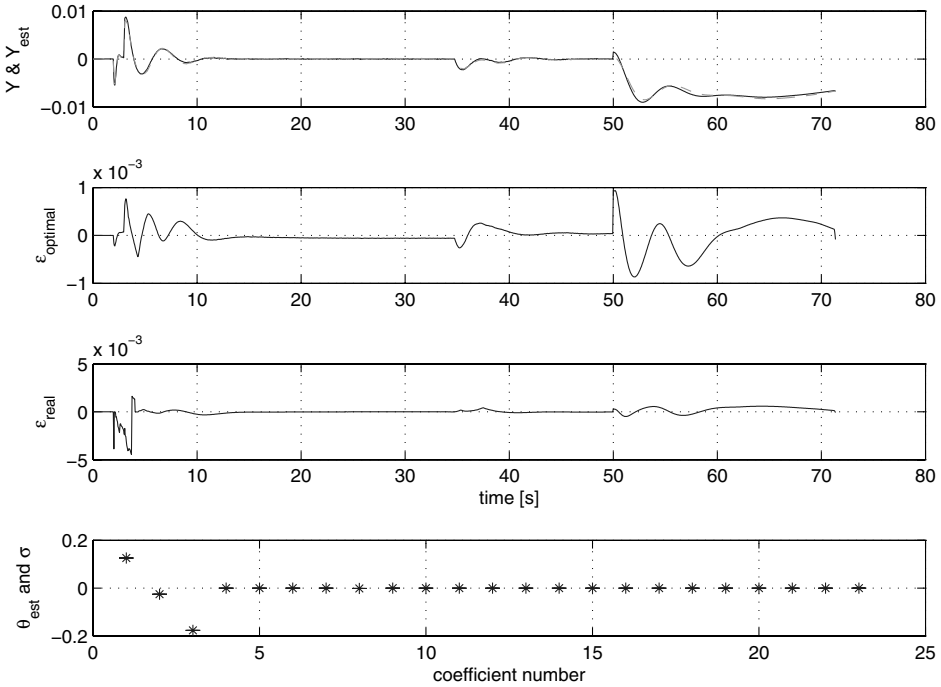

Fig. 16 Results of AROLS over complete time span for C_n. (Solid lines denote true and dashed lines denote final AROLS result.)

failure, as can be observed in this figure. This confirms the absence of any need for structure selection, as already observed in the previous results of this third application example.

V. Computational Efficiency and Real-Time Application

As can be observed from the working principle in Sec. III, AROLS is a recursive algorithm. This makes it suitable for online applications. However, real-time applicability depends on computational efficiency.

Several measures have been taken to make this algorithm computationally efficient. Adding data for every time step results in a stepwise growing data matrix Φ. However, its orthogonal decomposition results in a stepwise growing orthogonal **Q** matrix and a fixed-size triangular **R** matrix. Therefore, the computations have been optimized by making exclusive use of the triangular **R** matrix, which contains all the necessary information for the AROLS algorithm. In this way, the computational load is independent of the time instant. Moreover, the structure selection phase is restricted to the time span in which it is useful by considering a stopping criterion in step 3 and a starting criterion in step 8 in the working principle in

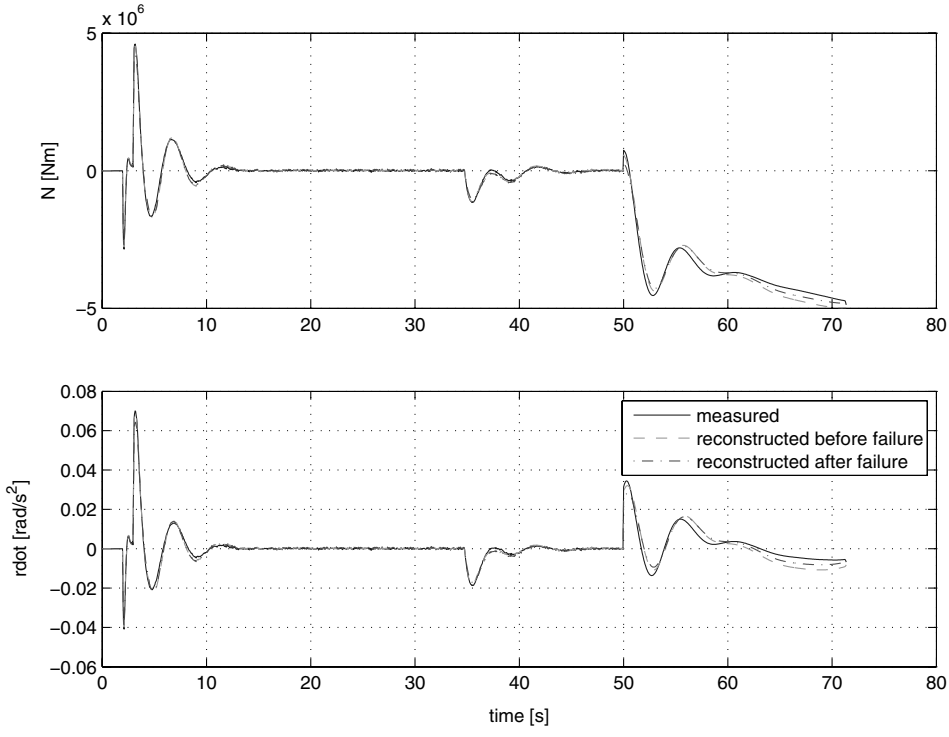

Fig. 17 Reconstruction of the yaw acceleration $\dot{r}$ with the SSPE result.

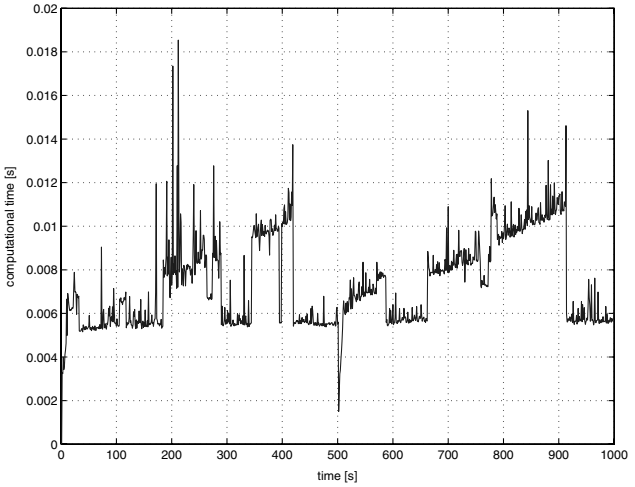

Fig. 18 Computational load of AROLS for every time step applied on a general data set.

Sec. III. In this way, computational efficiency is enhanced, as can be observed in Fig. 18. In this figure, the computational time of AROLS is presented for the calculations for every time step applied on a general data set, in which reinitialization occurs at $t = 500$ s. Structure selection is applied in specific intervals; namely, at $t = 200$–300 s, around $t = 400$ s, at $t = 500$–600 s, and at $t = 700$–900 s. The computational load caused by the structure selection steps (priority ranking, adding, and evaluating) is clearly visible in these time spans. Only relative comparisons of computational time values are useful here, because they reflect the computational load in the MATLAB® environment. It is expected that translation of the algorithm into C code will significantly improve the computational load, such that it will be real-time applicable to perform the calculations at frequencies ranging from 20–100 Hz on a PC with a Pentium 4 processor.

VI. Conclusions

Initial simulation results have shown that AROLS is a suitable new algorithm to develop an aerodynamic model structure and to estimate the model parameter values. The nature of the AROLS algorithm provides a protection against overfitting and thus avoids unnecessary complex models. This is an important advantage in order to minimize computational load. Moreover, possible collinearities between the regressors are dealt with, which is especially useful for situations in which there are a lot of (coupled) control surfaces. Finally, the structure selection and regression algorithm is made adaptive, so that it is reconfigurable for sudden, as well as gradual, changes in the aerodynamic model structure as a consequence of aerodynamic damage.

The performance of this algorithm has been evaluated on a high-fidelity Boeing 747 simulation model called RECOVER, which includes a realistic engine separation failure, inspired and validated by means of the DFDR readings from El Al flight 1862, which crashed in Amsterdam in 1992.

This approach works well for changes in the aerodynamic model structure. As a next step, there is also interest in taking into account the mass property changes in the aircraft model in order to increase the set of failures, which can be dealt with by this routine. In this way, a recursive model structure selection and parameter identification algorithm is obtained, which can be used in a subsequent stage for a model-based control algorithm (such as ANDI) in order to achieve FTFC.

Acknowledgments

This research was supported by the Dutch Technology Foundation under project number 06515. The authors thank Hafid Smaili and Jan Breeman from the National Aerospace Laboratory/NLR for providing the RECOVER simulation model.

References

[1] Dutoi, B., Richards, N., Gandhi, N., Ward, D., and Leonard, J., "Hybrid Robust Control and Reinforcement Learning for Optimal Upset Recovery," AIAA Guidance, Navigation, and Control Conference and Exhibit, AIAA Paper 2008-6502, Aug. 2008.

[2] Litt, J., and Guo, T., "Fast Thrust Response for Improved Flight/Engine Control Under Emergency Conditions," AIAA Guidance, Navigation, and Control Conference and Exhibit, AIAA Paper 2008-6503, Aug. 2008.

[3] Boskovic, J., Knoebel, N., Mehra, R., and Gregory, I., "An Integrated Approach to Damage Accommodation in Flight Control," AIAA Guidance, Navigation, and Control Conference and Exhibit, AIAA Paper 2008-6504, Aug. 2008.

[4] Tang, L., Roemer, M., Bharadwaj, S., and Belcastro, C., "An Integrated Health Assessment and Fault Contingency Management System for Aircraft," AIAA Guidance, Navigation, and Control Conference and Exhibit, AIAA Paper 2008-6505, Aug. 2008.

[5] Chang, B., Kwatny, H., Belcastro, C., and Belcastro, C., "Aircraft Loss-of-Control Accident Prevention: Switching Control of the GTM Aircraft with Elevator Jam Failures," AIAA Guidance, Navigation, and Control Conference and Exhibit, AIAA Paper 2008-6507, Aug. 2008.

[6] Bosworth, J., "Flight Results of the NF-15B Intelligent Flight Control System (IFCS) Aircraft with Adaptation to a Longitudinally Destabilized Plant," AIAA Guidance, Navigation, and Control Conference and Exhibit, AIAA Paper 2008-6985, Aug. 2008.

[7] Johnson, E., Calise, A. J., and De Blauwe, H., "In Flight Validation of Adaptive Flight Control Methods," AIAA Guidance, Navigation, and Control Conference and Exhibit, AIAA Paper 2008-6989, Aug. 2008.

[8] Lombaerts, T., Huisman, H., Chu, Q., Mulder, J., and Joosten, D., "Nonlinear Reconfiguring Flight Control Based on On-Line Physical Model Identification," *Journal of Guidance, Control, and Dynamics*, Vol. 32, No. 3, May–June 2009, pp. 727–748. doi:10.2514/1.40788

[9] Sonneveldt, L., van Oort, E., Chu, Q., and Mulder, J., "Nonlinear Adaptive Trajectory Control Applied to an F-16 Model," *Journal of Guidance, Control, and Dynamics*, Vol. 32, No. 1, Jan.–Feb. 2009, pp. 25–39. doi:10.2514/1.38785

[10] Maciejowski, J., and Jones, C., "MPC Fault Tolerant Flight Control Case Study: Flight 1862," *International Federation of Automatic Control on Safe Process Conference*, Elsevier, New York, 2003, pp. 119–124.

[11] Joosten, D., van den Boom, T., and Lombaerts, T., "Computationally Efficient Use of MPC and Dynamic Inversion for Reconfigurable Flight Control," AIAA Guidance, Navigation, and Control Conference and Exhibit, AIAA Paper 2008-7431, Aug. 2008.

[12] Murphy, P., and Klein, V., "Transport Aircraft System Identification from Wind Tunnel Data," AIAA Atmospheric Flight Mechanics Conference and Exhibit, AIAA Paper 2008-6202, Aug. 2008.

[13] Morelli, E., and Smith, M., "Real-Time Dynamic Modeling: Data Information Requirements and Flight Test Results," *Journal of Aircraft*, Vol. 46, No. 6, 2009, pp. 1894–1905. doi:10.2514/1.40764

[14] Song, Y., Campa, G., Napolitano, M. R., Seanor, B., and Perhinsch, M., "Online Parameter Estimation Techniques Comparison Within a Fault Tolerant Flight Control System," *Journal of Guidance, Control, and Dynamics*, Vol. 25, No. 3, May–June 2002, pp. 528–537. doi:10.2514/2.4913

[15] Ward, D., Monaco, J., and Bodson, M., "Development and Flight Testing of a Parameter Identification Algorithm for Reconfigurable Control," *Journal of Guidance, Control, and Dynamics*, Vol. 21, No. 6, Nov.–Dec. 1998, pp. 948–956. doi:10.2514/2.4329

[16] Lombaerts, T., Chu, Q., Mulder, J., and Joosten, D., "Real Time Damaged Aircraft Model Identification for Reconfiguring Control," AIAA AFM Conference and Exhibit, AIAA Paper 2007-6717, Aug. 2007.

[17] Lombaerts, T., Chu, Q., Mulder, J., and Joosten, D., "Flight Control Reconfiguration Based on Online Physical Model Identification and Nonlinear Dynamic Inversion," AIAA GNC Conference and Exhibit, AIAA Paper 2008-7435, Aug. 2008.

[18] Stroosma, O., Smaili, H., Lombaerts, T., and Mulder, J., "Piloted Simulator Evaluation of New Fault-Tolerant Flight Control Algorithms for Reconstructed Accident Scenarios," AIAA GNC Conference and Exhibit, AIAA Paper 2008-6534, Aug. 2008.

[19] Edwards, C., Lombaerts, T., and Smaili, M., *Fault Tolerant Control: a Benchmark Challenge*, Lecture Notes in Control and Information Sciences, Springer–Verlag, New York, 2008.

[20] Draper, N., and Smith, H., *Applied Regression Analysis*, Wiley, New York, 1981.

[21] Klein, V., Batterson, J., and Murphy, P., "Determination of Airplane Model Structure From Flight Data by Using Modified Stepwise Regression," NASA TP 1916, Oct. 1981.

[22] Vathsal, E., Sarkar, A., and Umakant, J., "Nonlinear Modeling and Roll Derivatives Estimation From Flight Data Using OLS," AIAA Atmospheric Flight Mechanics Conference and Exhibit, AIAA Paper 2004-5068, Aug. 2004.

[23] Morelli, E., "Nonlinear Aerodynamic Modeling using Multivariate Orthogonal Functions," AIAA Atmospheric Flight Mechanics Conference, AIAA Paper 1993-3636, Aug. 1993.

[24] Morelli, E., "Global Nonlinear Aerodynamic Modeling Using Multivariate Orthogonal Functions," *Journal of Aircraft*, Vol. 32, No. 2, March–April 1995, pp. 270–277.
doi:10.2514/3.46712

[25] Morelli, E. A., "Global Nonlinear Parametric Modeling with Application to F-16 Aerodynamics," *Proceedings of the American Control Conference*, International Federation of Automatic Control, Laxenburg, Austria, June 1998, pp. 997–1001.

[26] Klein, V., and Morelli, E. A., *Aircraft System Identification, Theory, and Practice*, AIAA Education Series, AIAA, Reston, VA, 2006, pp. 141–158.

[27] Barron, A. R., "Predicted Squared Error: a Criterion for Automatic Model Selection," *Self-Organizing Methods in Modeling*, edited by S. J. Farlow, Vol. 54, Marcel Dekker, New York, 1984, pp. 87–103.

[28] Mulder, J., "Design and Evaluation of Dynamic Flight Test Manoeuvers," Ph.D. Thesis, Aerospace Engineering, Delft Univ. of Technology, Delft, The Netherlands, 1986.

[29] Luo, W., and Billings, S., "Adaptive Model Selection and Estimation for Nonlinear Systems Using a Sliding Data Window," *Signal Processing*, Vol. 46, No. 2, 1995, pp. 179–202.
doi:10.1016/0165-1684(95)00081-N

[30] Luo, W., Billings, S., and Tsang, K., "On-Line Structure Detection and Parameter Estimation with Exponential Windowing for Nonlinear Systems," *European Journal of Control*, Vol. 2, Sept. 1996, pp. 291–304.

[31] Luo, W., and Billings, S., "Structure Selective Updating for Nonlinear Models and Radial Basis Function Neural Networks," *International Journal of Adaptive Control and Signal Processing*, Vol. 12, No. 4, 1998, pp. 325–345.
doi:10.1002/(SICI)1099-1115(199806)12:4<325::AID-ACS492>3.0.-CO;2-Q

[32] Fung, C., Billings, S., and Luo, W., "On-Line Supervised Adaptive Training Using Radial Basis Function Networks," *Neural Networks*, Vol. 9, No. 9, 1996, pp. 1597–1617.
doi:10.1016/S0893-6080(96)00024-X

[33] Chen, S., Billings, S., and Luo, W., "Orthogonal Least Squares Methods and Their Application to Non-Linear System Identification," *International Journal of Control*, Vol. 50, No. 5, 1989, pp. 1873–1896.
doi:10.1080/00207178908953472

[34] Miller, A. J., *Subset Selection in Regression*, CRC Press, Boca Raton, FL, 2002.

[35] Akaike, H., "Fitting Autoregressive Models for Prediction," *Annals of the Institute of Statistical Mathematics*, Vol. 21, No. 1, 1969, pp. 243–247.
doi:10.1007/BF02532251

[36] Akaike, H., "A New Look at the Statistical Model Identification," *IEEE Transactions on Automatic Control*, Vol. 19, No. 6, Dec. 1974, pp. 716–723.
doi:10.1109/TAC.1974.1100705

[37] Akaike, H., "Stochastic Theory of Minimal Realization," *IEEE Transactions on Automatic Control*, Vol. 19, No. 6, Dec. 1974, pp. 667–674.
doi:10.1109/TAC.1974.1100707

[38] Schwarz, G., "Estimating the Dimension of a Model," *Annals of Statistics*, Vol. 14, No. 3, 1978, pp. 416–464.
doi:10.1214/aos/1176344136

[39] Smaili, M., Breeman, J., Lombaerts, T., and Joosten, D., A Simulation Benchmark for Integrated Fault Tolerant Flight Control Evaluation, AIAA Modeling and Simulation Technologies Conference and Exhibit, AIAA Paper 2006-6471, 2006.

[40] Smaili, M., Breeman, J., and Lombaerts, T., "A Simulation Benchmark for Aircraft Survivability Assessment," 26th International Congress of the Aeronautical Sciences, International Council of the Aeronautical Sciences Paper 2008-9.3.2, Stockholm, 2008.

[41] Marcos, A., and Balas, G., "A Boeing 747-100/200 Aircraft Fault Tolerant and Fault Diagnostic Benchmark," Univ. of Minnesota TR AEM-UoM-2003-1, Minneapolis, MN, June 2003.

[42] Szaszi, I., Ganguli, S., Marcos, A., Balas, G. J., and Bokor, J., "Application of FDI to a Nonlinear Boeing 747 Aircraft," *Proceedings of the 10th Mediterranean Conference on Control and Automation*, IEEE Publ., Piscataway, NJ, July 2002.

[43] Chu, Q., "Lecture Notes AE4-394," *Modern Flight Test Technologies and System Identification*, Delft Univ. of Technology, Delft, The Netherlands, 2007.

[44] Laban, M., "On-Line Aircraft Aerodynamic Model Identification," Ph.D. Thesis, Delft Univ. of Technology, Delft, The Netherlands, May 1994.

[45] Mulder, J., Chu, Q., Sridhar, J., Breeman, J., and Laban, M., "Non-Linear Aircraft Flight Path Reconstruction Review and New Advances," *Progress in Aerospace Sciences*, Vol. 35, No. 7, 1999, pp. 673–726.
doi:10.1016/S0376-0421(99)00005-6

[46] Jategaonkar, R., *Flight Vehicle System Identification: A Time Domain Methodology*, Vol. 216, Progress in Astronautics and Aeronautics Series, 1st ed., AIAA, Reston, VA, 2006.

[47] Morelli, E., "Real-Time Parameter Estimation in the Frequency Domain," *Journal of Guidance, Control, and Dynamics*, Vol. 23, No. 5, 2000, pp. 812–818.
doi:10.2514/2.4642

[48] Chu, Q., Mulder, J., and Sridhar, J., "Decomposition of Aircraft State and Parameter Estimation Problems," *Proceedings of the 10th IFAC Symposium on System Identification*, Vol. 3, International Federation of Automatic Control, Laxenburg, Austria, 1994, pp. 61–66.

[49] Hamel, P. G., and Jategaonkar, R. V., "Evolution of Flight Vehicle System Identification," *Journal of Aircraft*, Vol. 33, No. 1, Jan.–Feb. 1996, pp. 9–28.
doi:10.2514/3.46898

[50] Weiss, S., Friehmelt, H., Plaetschke, E., and Rohlf, D., "X-31A System Identification Using Single-Surface Excitation at High Angles of Attack," *Journal of Aircraft*, Vol. 33, No. 3, May–June 1996, pp. 485–490.
doi:10.2514/3.46970